OXFORD

SOT | Society of Toxicology
www.toxsci.oxfordjournals.org

TOXICOLOGICAL SCIENCES, 167(1), 2019, 58–76

doi: 10.1093/toxsci/kfy218
Advance Access Publication Date: August 31, 2018
Research Article

Functional and Mechanistic Neurotoxicity Profiling Using Human iPSC-Derived Neural 3D Cultures

Oksana Sirenko,[*,1] Frederick Parham,[†] Steven Dea,[‡] Neha Sodhi,[‡] Steven Biesmans,[‡] Sergio Mora-Castilla,[‡] Kristen Ryan,[†] Mamta Behl,[†] Grischa Chandy,[*] Carole Crittenden,[*] Sarah Vargas-Hurlston,[*] Oivin Guicherit,[‡] Ryan Gordon,[‡] Fabian Zanella,[‡] and Cassiano Carromeu[‡,1]

[*]Molecular Devices LLC, San Jose, California 95134; [†]Division of the National Toxicology Program, National Institute of Environmental Health Sciences, Research Triangle Park, North Carolina; and [‡]StemoniX, Inc, Maple Grove, Minnesota 55311

[1]To whom correspondence should be addressed at 3860 N First Street, San Jose, CA 95134 1.408.548.6051. E-mail: oksana.sirenko@moldev.com and E-mail: cassiano.carromeu@stemonix.com.

ABSTRACT

Neurological disorders affect millions of people worldwide and appear to be on the rise. Whereas the reason for this increase remains unknown, environmental factors are a suspected contributor. Hence, there is an urgent need to develop more complex, biologically relevant, and predictive *in vitro* assays to screen larger sets of compounds with the potential for neurotoxicity. Here, we employed a human induced pluripotent stem cell (iPSC)-based 3D neural platform composed of mature cortical neurons and astrocytes as a model for this purpose. The iPSC-derived human 3D cortical neuron/astrocyte co-cultures (3D neural cultures) present spontaneous synchronized, readily detectable calcium oscillations. This advanced neural platform was optimized for high-throughput screening in 384-well plates and displays highly consistent, functional performance across different wells and plates. Characterization of oscillation profiles in 3D neural cultures was performed through multi-parametric analysis that included the calcium oscillation rate and peak width, amplitude, and waveform irregularities. Cellular and mitochondrial toxicity were assessed by high-content imaging. For assay characterization, we used a set of neuromodulators with known mechanisms of action. We then explored the neurotoxic profile of a library of 87 compounds that included pharmaceutical drugs, pesticides, flame retardants, and other chemicals. Our results demonstrated that 57% of the tested compounds exhibited effects in the assay. The compounds were then ranked according to their effective concentrations based on *in vitro* activity. Our results show that a human iPSC-derived 3D neural culture assay platform is a promising biologically relevant tool to assess the neurotoxic potential of drugs and environmental toxicants.

Key words: 3D neural cultures; calcium oscillations; neurotoxicity; flame retardants; pesticides; polyaromatic hydrocarbons; iPSC.

This article is published as part of the NTP Neurotoxicology Screening Strategies Initiative.

There is an increasing need for more predictive *in vitro* models to test compounds for their toxicological effects on the central nervous system (CNS) (Judson *et al.*, 2009a). In addition, neurotoxicity is a major reason for attrition in the final stages of a drug development pipeline (Jordan and Wilson, 2004; Wijdicks, 2001). Current approaches for neurotoxic evaluation of chemicals rely mostly on animal models, which have limitations related to throughput, cost, and translatability to human CNS. Therefore, many incentives exist to facilitate the development of a more relevant human toxicological screening platform with improved *in vitro* predictability (Betts, 2013; Marchan *et al.*, 2013; Tice *et al.*, 2013). Morphological neurite outgrowth assays were previously used to explore the ability of compounds to adversely affect the developing nervous system (Harrill *et al.*, 2013;

Radio and Mundy, 2008; Ryan *et al.*, 2016; Sirenko *et al.*, 2016). Multi-electrode arrays (MEAs) have also been utilized for neurotoxicity evaluation (Frank *et al.*, 2017; Valdivia *et al.*, 2014). Finally, it has been shown that changes in intracellular calcium levels can be used as an important biomarker to investigate the effects of compounds on network physiology (Cohen *et al.*, 2008; Dravid and Murray, 2004; Kuijlaars *et al.*, 2016). Calcium oscillations are dependent on an influx of extracellular calcium through L-type voltage-gated calcium channels, the rising phase of each calcium spike is coincident with a brief burst of action potentials (Robinson *et al.*, 1993; Wang and Gruenstein, 1997). Intracellular calcium levels can be used as a screening tool to evaluate neurotoxic effects of compounds, including seizurogenic effects (Cao *et al.*, 2012; Smetters *et al.*, 1999; Wang and Gruenstein, 1997; Wong, 1998), as well as for testing antiepileptic drugs (Pacico and Mingorance-Le Meur, 2014). Calcium imaging has also been useful in revealing properties of the activity of neural networks *in vitro*, albeit in a different way than the MEA. Whereas MEAs measure the field potential activity of the cells, calcium imaging measures changes in intracellular calcium levels that correlate with the action potential (Shew *et al.*, 2010; Wong, 1998). Importantly, the calcium assay can be fully automated in a high-throughput fashion, making it useful for neurotoxicity screenings, target validation, or phenotypic drug screenings.

In this study, we describe phenotypic assays for toxicity assessment using human iPSC-derived 3D neural cultures. The 3D culture of human iPSC-derived neural cells is composed of cortical glutamatergic and GABAergic neurons and astrocytes from a single donor source. There has been growing interest in using 3D cell models containing multiple cell types for studying complex biology and tissue architecture (Camp *et al.*, 2015; Chang and Hughes-Fulford, 2009; Lancaster and Knoblich, 2014; Luo *et al.*, 2016; Ramsden *et al.*, 2014; Renner *et al.*, 2017) due to the ability of cell aggregates to organize and more closely recapitulate key aspects of the human tissue (Hartley and Brennand 2016; Jorfi *et al*, 2018; Hendriks *et al.*, 2012; Kelm and Fussenegger, 2004). Importantly, the *in vitro* model described in this manuscript enables detection of consistent spontaneous calcium oscillations and can be used in high-throughput multiwell format for screening of potential hazardous effects of chemicals.

We characterized phenotypic responses to various compounds by monitoring the impact on the frequency and pattern of the spontaneous calcium oscillations. In parallel, high content confocal imaging of the spheroids was used to characterize cellular viability in response to compound treatment. The method was optimized for a high-throughput format (384-well).

First, we characterized the method and evaluated the cellular responses to a set of compounds including 10 well-characterized neuroactive agents and 22 reported neurotoxic substances. To test the feasibility of this approach to identify and prioritize chemicals according to their relative neurotoxicity, we next screened a diverse selection of 87 chemicals that contain representative examples of compounds from various environmentally relevant and potentially neurotoxic groups, including pesticides (Shafer and Meyer, 2004; Soderlund *et al.*, 2002), brominated and organophosphorus flame retardants (Dingemans *et al.*, 2011; Hendriks and Westerink, 2015), and polycyclic aromatic hydrocarbons (PAHs) (Kaufman *et al.*, 1992; Zafiropoulos *et al.*, 2014; Zhang *et al.*, 2013). Using techniques previously developed to characterize alterations in spontaneous calcium oscillations (Grimm *et al.*, 2015; Sirenko *et al.*, 2017), we applied a multi-parametric quantification approach to evaluate concentration-dependent effects of these diverse chemicals on neuronal physiology. Finally, quantitative concentration-response assessments of various kinetic and image-based phenotypes provided benchmark concentrations (BMCs) that were utilized as measures of toxicity for bioactivity profiling and compound ranking.

MATERIALS AND METHODS

Human iPSC-derived 3D cortical neuron/astrocyte co-cultures. Pre-plated 3D human cortical neural co-cultures were obtained from StemoniX, Inc in the form of the StemoniX microBrain 3D Assay Ready 384-Plate product (StemoniX No. BSARX-AA-0384, Maple Grove, Minnesota). The product is delivered as ready-to-use 3D neural cultures in a 384-well format, shipped at room temperature. Upon arrival, media change was performed according to manufacturer's instructions (described in detail in the Cell culture section). Each well of the plate contains a single, free-floating human iPSC-derived cortical 3D neural culture generated from Neural Progenitor Cells (NPCs) obtained from a single human donor source.

Chemicals. Hoechst 33342, MitoTracker Orange, and Calcein AM Green were purchased from Invitrogen (Carlsbad, California). FLIPR Calcium 6 Dye was from Molecular Devices (San Jose, California). All other compounds, with the exception of the Chemical Library, were purchased from Sigma Co (St. Louis, Missouri) or Tocris Bioscience Co (Bristol, U.K.).

Chemical library. The compound library used in this study comprised 87 unique chemicals provided by the National Toxicology Program. The compound set was selected to reflect a diversity of chemicals from various classes, including pharmaceutical drugs ($n = 19$), pesticides ($n = 16$), flame retardants ($n = 15$), and PAHs (PAHs, $n = 17$). Several metals (lead, mercury) and other categories of chemicals (eg, acrylamide, bisphenol) that could be categorized as 'industrial' were also included in the library ($n = 15$). The library contains four compounds (deltamethrin, triphenyl phosphate, methyl mercuric(II) chloride, saccharin) in duplicate for a total of 91 compounds tested. Assay-specific positive neurotoxic (methyl mercury, berberine chloride) and non-toxic (saccharin, D-glucitol, acetaminophen, acetylsalicylic acid, L-ascorbic acid) substances were included in the library. The list of compounds is shown in Supplementary Table 1. Additional information regarding the NTP chemical library can be found in Behl *et al.* (in preparation). 20 mM stock solutions of all chemicals were prepared in cell-culture grade dimethyl sulfoxide (DMSO, Sigma Co) and stored at −20°C; few compounds had different stock concentrations due to solubility limitations (see Supplementary Table 1). Vehicle controls ($n = 20$; DMSO concentration 0.15%) and untreated controls were included on each assay plate and were used for normalization of plate-specific phenotypic readouts.

Cell culture. microBrain 3D Assay Ready 384-Well plates were shipped overnight at ambient conditions. Upon receipt, plates were processed according to detailed manufacturer's instruction included with the product. Briefly, after unpacking, plates were centrifuged for 10 min at 200 rcf (Sorvall centrifuge) and then inspected using a light microscope to ensure the presence of a single spheroid in each well, and plate exteriors were decontaminated with 70% ethanol. After unsealing, the medium was changed (½ volume, 3 times) using BrainPhys Neuronal Medium SM1 Kit (StemCell Technologies, No. 05792, Vancouver,

BC, Canada) supplemented with 20 ng/ml of recombinant human BDNF (StemCell Technologies, No. 78005), 20 ng/ml of GDNF (StemCell Technologies, No. 78058), and 1X Penicillin-Streptomycin (GE Healthcare Life Sciences). Finally, plates were placed into the incubator (37°C) for 7 days. Half media changes were performed every second day using the BrainPhys Neuronal Medium SM1 Kit with BDNF, GDNF, and Penicillin-Streptomycin. Compound treatments were performed at multiple time points using replacement of ½ volume of media containing compounds. The final concentration of DMSO was 0.15%, except for the 100 μM concentration, which contained 0.5% DMSO.

Characterization of gene expression. RNA from 3D neural cultures was extracted using the RNeasy Plus Mini Kit (Qiagen, Hilden, Germany) following the manufacturer's recommendations. RNA was suspended in 50 μl of RNase-free water. For each sample, concentration and A_{260}/A_{280} ratio were determined (all samples had ratios equal to or more than 1.8). As a positive control we used the FirstChoice Human Brain Total RNA (Thermo Fisher Scientific, Waltham, Massachusetts). As a negative control we extracted RNA from the undifferentiated human iPSC line used to generate the 3D neural cultures (StemoniX). Briefly, source iPSCs were grown in mTeSR media (StemCell Technologies) and passaged manually at 80% confluence to Matrigel (Corning) coated dishes (RNA was extracted using the RNeasy kit method described above). RT^2 Profiler PCR Arrays (Qiagen) for neurotransmitter receptors (PAHS-060Z) and neuronal ion channels (PAHS-036Z) were used to characterize the neuronal profile of the 3D neural cultures. A total of 500 ng of RNA was used per sample for cDNA synthesis. All reactions for the qPCR were done following the manufacturer's recommendations. Gene expression analysis was done using the Data Analysis Center from Qiagen. Briefly, we used geometric mean normalization with the 5 housekeeping genes present on the PCR array to calculate the $\Delta\Delta C_T$. For each gene, fold change was calculated using the formula: Fold change $= 2^{(-\Delta\Delta CT)}$.

Calcium oscillation assay. The intracellular Ca^{2+} oscillations in 3D neural cultures were assessed using the FLIPR Calcium 6 Kit (Molecular Devices LLC, San Jose, California) as described previously in Grimm *et al.* (2015) and Sirenko *et al.* (2013b). Calcium dye interacts with intracellular calcium and fluorescence changes according to increased or decreased calcium concentration. Kinetics of intracellular Ca^{2+} oscillations were determined as fluorescence intensity at 515–575 nm following excitation at 470–495 nm for 10 min at a frequency of 3 Hz using the FLIPR Tetra High-Throughput Cellular Screening System (Molecular Devices LLC). The exposure time per read was 0.4 s, the gain was set to 2000, and the excitation intensity was set to 30%. The instrument temperature was kept at a constant 37°C. For acute exposure to compounds, cells were pre-loaded with Calcium 6 Dye for 2 h prior to compound addition. Baseline for calcium oscillations without compounds was measured prior to compound addition. Then compounds were added, and effects on calcium oscillations were measured after 60 min of exposure. For 24 h or 72 h exposure experiments, cells were exposed to chemicals at appropriate concentrations for 22 or 70 h prior to the addition of the Ca^{2+}-reagent; the Calcium 6 Dye (4× concentration) was added for an additional 2 h, with the extra addition of compounds to compensate for the volume change. For quantitative data evaluation, representative descriptors, such as peak count (per 10 min), average peak amplitude, average peak width (at 10% amplitude), average peak spacing (time between peaks), average peak rise time (from 10% to 90% amplitude), and average peak decay time (from 90% to 10% amplitude), were automatically derived using the ScreenWorks Peak Pro (4.2) software package (Molecular Devices LLC). Cell viability after 24 or 72 h of treatment was assessed using quantitative imaging of viable cells following staining with Calcein AM and MitoTracker Orange CMTMRos as described below. Individual compounds were tested across 6–7 concentrations, typically in triplicates. Compounds from chemical library were tested in duplicates, across 6 concentrations; whereas library screen was repeated 2 times.

Multi-electrode array electrophysiology. To compare calcium oscillations with electrical response, 4-week-old 3D neural cultures were obtained and processed as described in the Cell culture section. After processing, individual spheroids were plated on 96-well MEAs (Axion Biosystems, Atlanta, Georgia). Briefly, the MEA plate was coated with 50 μg/ml of Poly-L-Ornithine for 4 h at 37°C, washed 2 times with PBS, and coated with 10 μg/ml of laminin (in PBS) for another 4 h at 37°C. After removing the laminin, one 3D neural culture was plated in each well of the MEA plate in BrainPhys Neuronal Medium SM1 Kit (StemCell Technologies) supplemented with 20 ng/ml of BDNF (StemCell Technologies, No. 78005), 20 ng/ml of GDNF (StemCell Technologies, No. 78058), and 1X Hyclone Penicillin-Streptomycin (GE Healthcare Life Sciences, No. SV30010). MEA plates were incubated for 2 weeks, and half-volume media changes were performed every other day. Careful manipulation was used to avoid detachment during media changes. After 2 weeks, spontaneous neuronal activity was recorded using the Maestro MEA system (Axion Biosystems). Effects of select chemicals were tested in the assay in duplicate, after treatment for 60 min.

Immunostaining. To analyze the spheroid cellular content, 3D neural cultures were fixed with 4% Paraformaldehyde (PFA) solution in PBS for 20 min followed by washing 5 times in half-volume with PBS to remove residual PFA. The cells were permeabilized with 0.2% Triton X-100 diluted in Odyssey Blocking Buffer (Li-Cor, Lincoln, Nebraska) for 15 min at room temperature. After discarding the permeabilization solution, the spheroids were then incubated with Odyssey Blocking Buffer for 4 h before addition of antibody. Three-dimensional neural cultures were incubated with primary antibodies diluted (1:1000) in Odyssey Blocking Buffer for 16 hr at 4°C under gentle agitation. After primary antibody incubation, spheroids were washed 8 times with 0.1% Tween-20 diluted in PBS. AlexaFluor secondary antibodies were diluted 1:500 in Odyssey Blocking Buffer and added to the spheroids. Hoechst nuclear dye was also added (1 μM). After incubating 1 h at room temperature, cells were washed 8 times with 0.1% Tween-20 diluted in PBS. The final wash was performed with PBS without Tween-20, and spheroids were imaged using the ImageXpress Micro Confocal High-Content Imaging System (Molecular Devices LLC).

3D imaging and analysis. For viability readouts, spheroids were stained and imaged live by adding 2× solution of Hoechst, Calcein AM, and MitoTracker Orange CMTMRos (3 μM, 1 μM, and 0.5 μM respectively, in PBS) and incubating at 37°C for 2 h. Spheroids were imaged using an automated confocal imaging system, the ImageXpress Micro Confocal system, with a 10× PlanFluor objective. The method for staining spheroids and acquisition settings for spheroid assays were described previously in Sirenko *et al.* (2015, 2016). Briefly, a Z-stack of 19 images

separated by 10–15 μm was acquired and analyzed using MetaXpress 6.2 Software (Molecular Devices). The automated analysis method first identified the spheroid and counted total number of cells using the nuclear stain. Then the number of live cells was identified by the presence of the Calcein AM signal, and the number of cells with intact mitochondria was detected by MitoTracker Orange staining. The number or % of positive cells can be used for viability assessment.

Concentration-response analysis for individual compounds. For the initial characterization of the effects of neuromodulators and the first limited set of neurotoxic compounds, we used standard methods for EC_{50} evaluation. EC_{50} values for the limited set of compounds were determined using 4-parameter curve fits via the SoftMax Pro 6 Software (Molecular Devices LLC). However, because some toxic compounds had not led to complete inhibition of peak counts even at the limits of their solubility, a different statistical approach was used for analysis of concentration responses for screening the library for calculation of effective concentrations.

Concentration-response analysis for chemical library screening. For quantitative toxicity profiling, we initially normalized phenotype and plate-specific readouts to their respective vehicle controls. Normalized data points were subsequently subjected to the Hill function fit using the model found in the tcpl R package (Filer *et al.*, 2017; Grimm *et al.*, 2015; Sirenko *et al.*, 2013a). Point-of-Departure (POD) values, herein defined as the concentration at which the fitted curve intersects three standard deviations above or below (depending on the phenotypic readout) the mean of the vehicle controls, were then derived from the curve parameters (Wignall *et al.*, 2014).

Assessment of assay variability. The integrity and replicability of all screening assays were assessed using a variety of quality controls. As a general measure for assay performance, we determined the coefficients of variation (%CV), herein defined as the ratio of one standard deviation and the means of the vehicle controls ($n = 24$) for calcium oscillation phenotypes after 24 h; the same method was used to obtain %CV for cellular and mitochondrial toxicity phenotypes. The inter-plate and intra-plate replicabilities for control samples for all readouts were assessed using comparison between different wells in one plate or comparison of control samples from different plates. In addition, concentration-responses for decrease in peak rates were compared between 2 experiments for 8 representative compounds. Correlation coefficients between data were calculated for all readouts. Finally, when screening the chemical library, the experiment was conducted two times using two different lots of cells. Therefore, there were 2 technical replicates and 2 biological replicates. The chemical selection included a list of positive and negative controls for the various phenotypes measured in this study.

RESULTS

A schematic of the overall experimental approach is shown in Figure 1.

Characterization of 3D Neural Cultures

The microBrain 3D neural culture platform comprises a 384-well plate with one spheroid per well (Figure 2A). Spheroid diameter was approximately 635 ± 32 μm with a coefficient of variation across the plate of 5.2% (Supplementary Figure 2A).

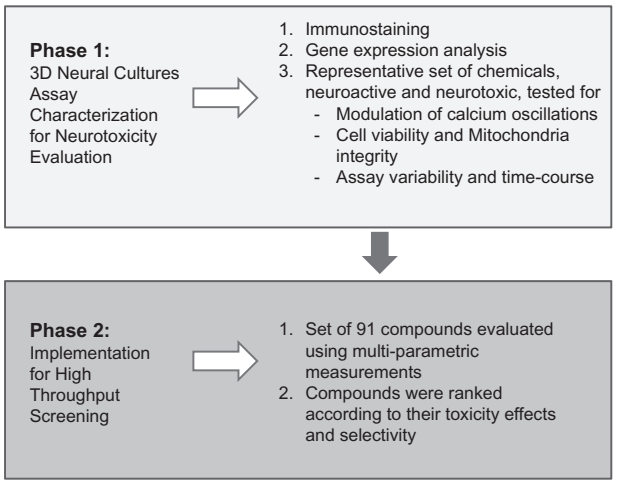

Figure 1. Phenotypic 3D neural cultures assay development and implementation workflow.

Staining of spheroids for MAP2 (Microtubule-associated protein 2) and GFAP (Glial fibrillary acidic protein) demonstrated that the neural network is composed of a balanced ratio of neurons and astrocytes (Figure 2B). Staining for Aquaporin 4 and Synapsin I markers confirmed the presence of these key neural markers in the system (Figs. 2C and 2D).

To further characterize neural identity, we performed qPCR analysis for a panel of ion channel and neurotransmitter receptor genes. Expression levels of 20 key neuronal genes in each of these categories are presented in Figures 3A and 3B. In addition, expression levels for the same genes are presented for a post-mortem human brain sample (Figs. 3A and 3B).

Calcium Oscillation Measurements in 3D Neural Cultures

The basal activity of the spontaneous calcium oscillations in the 3D neural cultures was assessed using a kinetic high-throughput system (FLIPR Tetra system). The cortical spheroids produced measurable, strong, and consistent spontaneous calcium oscillations across all 384-wells (Supplementary Figs. 1 and 2). The calcium oscillations were also observed and recorded at higher resolution using imaging methods (Supplementary Figure 1). Calcium oscillation patterns were analyzed using a variety of quantifiable readouts, including peak count, average peak amplitude, average peak spacing, and average peak width, as well as average rise and decay times (Supplementary Figure 3A). Spheroid calcium signaling across the plate is shown in Supplementary Figure 2B. For baseline readings, without compound addition, the coefficient of variation for peak count was 17.8% across a representative 384-well plate (data not shown) indicating consistent performance between different wells.

Effects of test compounds on changes in the pattern of calcium oscillations can be characterized in more detail using six quantitative descriptors of intracellular Ca^{2+} oscillations: peak count (for 10 min of recorded time), average peak amplitude, average peak width (at 10% of peak amplitude), average spacing between peaks, and peak rise and decay times (Supplementary Figure 3A). A similar approach was used previously for evaluation of calcium oscillations (Grimm *et al.*, 2015; Sirenko *et al.*, 2013a,b), and it was employed here to characterize and quantify the physiological responses of the neural platform in response to neurotoxic agents. It should be noted that we have not been able to demonstrate consistent and reproducible spontaneous

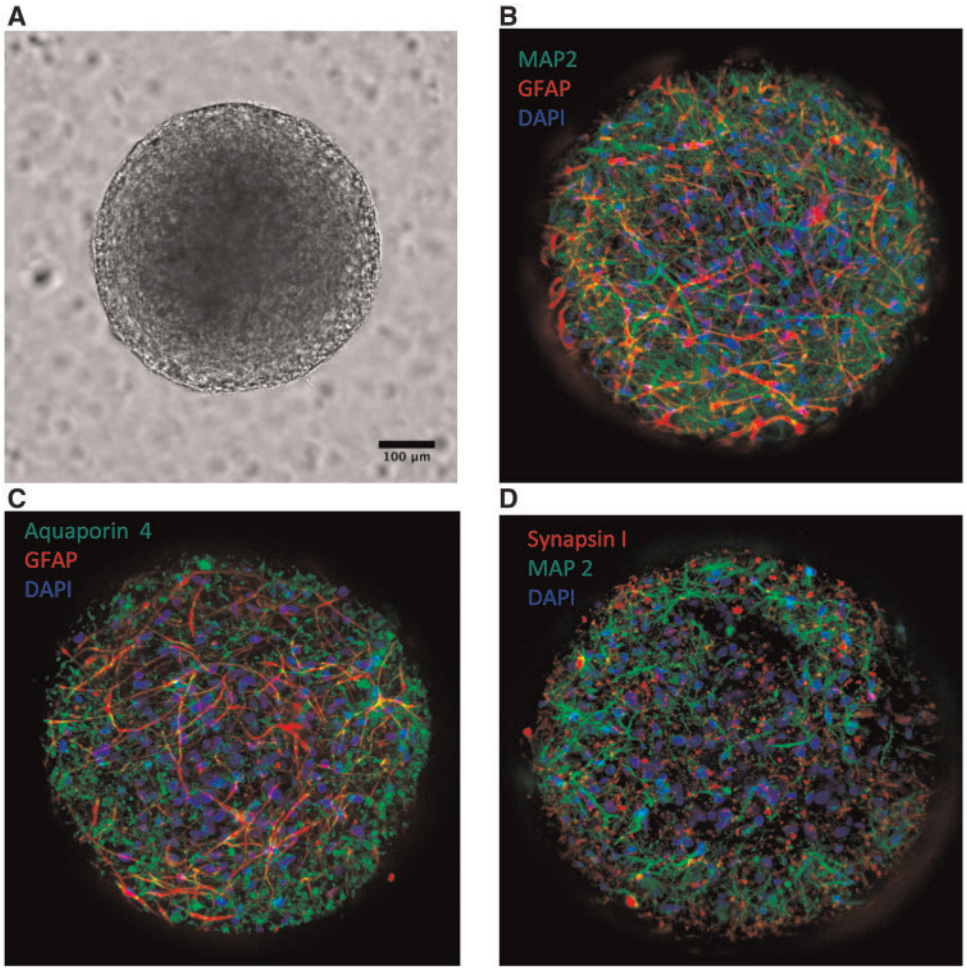

Figure 2. (A) Human iPSC-derived 3D neural culture spheroids, approximately 600 µm diameter, imaged with ImageXpress Micro Confocal system, 20x magnification, transmitted light. (B) Fluorescent images were taken after staining cells with marker-specific antibodies as described in Materials and Methods section. Images were taken using 20× objective in confocal mode. Spheroids are composed of a co-culture of active cortical neurons (identified by MAP2; green) and astrocytes (identified by GFAP; red). (C) Staining for Aquaporin 4 (green) showed the presence of mature GFAP-positive astrocytes. (D) Staining for Synapsin I (red) showed the presence of mature MAP2-positive neurons. B, C, and D show composite projection images of 3D neural cultures (30 images, 15 µm apart). Nuclei are stained with Hoechst 33342 (blue).

calcium oscillations using similarly cultured cells in a 2D plate format (data not shown).

To compare calcium oscillations with electrical behavior, 3D neural cultures were collected from 384-well plates and re-plated onto a microelectrode array (MEA) (Axion Biosystems) for electrophysiology measurements. The observed synchronized oscillatory behavior shown by coordinated neuronal bursting on multiple electrodes corroborates the activity observed in the calcium-based assay. Compared with DMSO treatment, several neuromodulators inhibited neural activity at concentration ranges $\leq$30 µM. (Supplementary Figs. 3B and 3C).

Evaluation of Functional Responses to a Selected Set of Compounds

To characterize the Ca^{2+} oscillation assay in the 3D neural cultures for neurotoxicity using the FLIPR Tetra System, we tested responses of a set of 32 compounds at concentrations ranging from 0.1 to 30 µM (with some up to 100 µM), including 10 well-characterized neuroactive agents (Table 1), 22 reported neurotoxic substances (Table 2), and 2 negative controls.

Abnormalities in the glutamate and GABA systems have been shown to lead to a variety of neurological disorders (Derecki *et al.*, 2010; Whitehouse *et al.*, 1982). Effects of neuroactive compounds were recorded and evaluated after 60 min of exposure. This set of neuroactive reference compounds includes several glutamatergic and GABAergic agonists and antagonists (Beattie *et al.*, 2000; Carroll *et al.*, 2001), as well as four pharmaceutical drugs: lidocaine, phenytoin, haloperidol, and lamotrigine (Goldsmith *et al.*, 2003; Seeman, 2002; Sheu and Lederer, 1985; Zafar *et al.*, 2012).

Examples of Ca^{2+} oscillation traces reflecting a diverse range of compound effects on 3D neural cultures are shown in Figure 4A. Concentration-response effects for peak count values are shown for selected compounds in Figure 4B. The calculated EC_{50} values, calculated from concentration responses, are presented in Table 1. Exposure to kainic acid, an agonist of the kainate receptor, produced an expected concentration-dependent pharmacological reaction indicating responsive stimulation of the excitatory glutamatergic system, as well as inhibition of the peak count above 3 µM (Figure 4B). One possibility for the observed inhibition at increased concentrations of kainic acid is the depletion of glutamate stocks at the synapses, or due to excessive activation of the glutamate receptors or glutamate

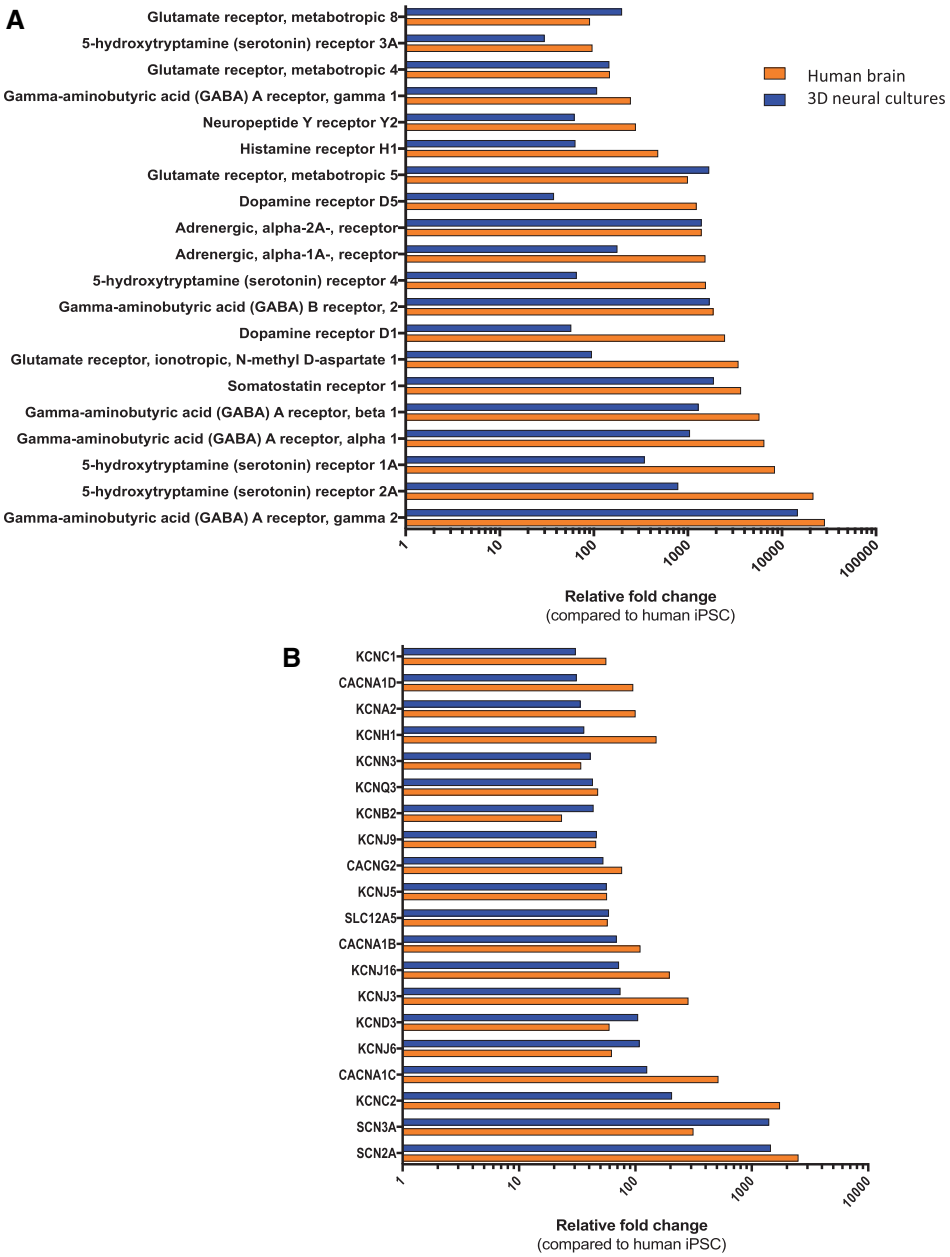

Figure 3. (A) Gene expression profiling for neurotransmitters receptors. (B) Gene expression profiling for ion channels. Data presented for 3D neural cultures samples and adult brain samples. Both values were normalized to iPSC cells. KCNC1 and others represent Potassium Voltage-Gated Channels; SCN2A and other represent Sodium Voltage-Gated Channels; CACNA1D represent L-type calcium channels.

receptor desensitization (Pérez-Gómez *et al.*, 2018). Treatment with CNQX, a glutamatergic inhibitor and AMPA/kainate receptor antagonist, or MK-801, an antagonist of the NMDA receptor, also led to a concentration-dependent decrease in peak counts and an increase in the distance between peaks and peak regularity (Figure 4B). As anticipated, GABA and the GABA receptor agonist baclofen inhibited the frequency of calcium oscillations. Pharmaceutical drugs lidocaine or haloperidol also led to modulation of pattern and subsequent inhibition of calcium oscillations (Figs. 4A and 4B).

Tested neuroactive compounds demonstrated concentration-dependent activity, from which their half maximal concentrations (EC_{50}) were determined. Table 1 presents the calculated EC_{50} values for compounds using the peak count readout and includes reference EC_{50} values for the same compounds previously determined in other *in vitro* assays (Arvanov *et al.*, 1997; Caeser *et al.*, 1999; Chou *et al.*, 2014; Coyne *et al.*, 2007; Crawford and Young, 1988; Galvez *et al.*, 2000; Goldsmith *et al.*, 2003; Huettner and Bean, 1988; King *et al.*, 1999; Larm *et al.*, 1996; Lee *et al.*, 2010; Login *et al.*, 1998; McCool *et al.*, 2003; Regan, 1996; Sheets and Hanck, 2003; Wong *et al.*, 1986; Zhao *et al.*, 2016). The results indicated that the calcium oscillations of iPSC-derived 3D neural cultures were sensitive to the known modulators of neural activity, confirming a direct link between the spontaneous calcium oscillations observed and neuronal activity.

Next, we tested a set of 22 compounds, which were selected based on results of our previous study (Ryan *et al.*, 2016) using a

Table 1. Effects of Selected Compounds

Compound	Mechanism of Action	IC_{50} (μM), This Study	Reference IC_{50} (μM)	References
Kainic acid	Agonist of kainate receptor	2.66	3; 20	Pérez-Gómez *et al.* (2018) and Larm *et al.* (1996)
MK-801	Antagonist of NMDA receptor	0.033	0.037	Wong *et al.* (1986) and Huettner and Bean (1988)
CNQX	Antagonist of AMPA/kainate receptor	2.05	0.3–1.5	Lee *et al.* (2010)
Muscimol	Agonist of $GABA_A$ receptor	0.021	0.47	Login *et al.* (1998) and King *et al.* (1999)
(R)-Baclofen	Agonist of $GABA_B$ receptor	0.45	0.70	Galvez *et al.* (2000)
GABA	Endogenous agonist of GABA receptor	5.93	7; 27	Coyne *et al.* (2007) and McCool *et al.* (2003)
Haloperidol	Antagonist of D2 dopamine receptor	0.13	0.037	Arvanov *et al.* (1997)
Lidocaine	Voltage-gated Na^+ channel blocker	9.47	5	Sheets and Hanck (2003)
Phenytoin (dilantin)	Voltage-gated Na^+ channel blocker	9.41	16	Zhao *et al.* (2016)
Lamotrigine isothionate	Voltage-gated Na^+ channel blocker	34.1	66	Zhao *et al.* (2016) and Caeser *et al.* (1999)

IC_{50} (concentration of an inhibitor where the response is reduced by half) reported to all compounds, with the exception of Kainic Acid, where the EC_{50} (concentration of compound that gives half-maximal response) is shown.

Table 2. Effects of Selected Compounds

EC_{50}, μM	Peak Count			Viability		
Compounds	1 h	24 h	72 h	1 h	24 h	72 h
Rotenone	0.03	0.03	0.03		95.3	98.8
Valinomycin	0.84	0.09	0.05			>100
Deltamethrin	1.20	0.22	0.42		>100[a]	>100
Berberine chloride	11.3	1.19	0.45			96.3
2-Ethylhexyl diphenyl phosphate (EHDP)	4.14	1.53	3.65			
Methyl mercuric(II) chloride	10.7	4.68	1.64			39.7
Tricresyl phosphate	7.65	3.01	2.95			
Isodecyl diphenyl phosphate	12.2	3.25	0.23			104
Dichlorodiphenyltrichloroethane (DDT)	23.2	3.37	3.37			
Dieldrin	19.5	3.43	8.89	>100	>100	>100
2,2′,4,4′,5-Pentabromodiphenyl ether (BDE-99)	No fit[b]	4.33	3.96	No fit	>100	>100
Diethylstilbestrol	15.1	11.5	21.4		>100	39.6
2,2′,4,4′-Tetrabromodiphenyl ether	36.1	11.9	1.21			
Triphenyl phosphate	18.7	14.1	14.2			>100
Tris(chloropropyl) phosphate (TCPP)	31.7	38.5	10.3			
Captan	[c]	42.7	104			
Lead (II) acetate trihydrate	[c]	82.4	14.5			64.9
1-Ethyl-3-methylimidazolium diethylphosphate	No fit	108	136			
2,3,7,8-Tetrachlorodibenzo-p-dioxin	No fit	No fit	6.03			
Benzo(a)pyrene	No fit	No fit	8.67			
Phenobarbital sodium salt	No fit	No fit	No fit			
Dibenz[a,c]anthracene	No fit	No fit	No fit			
Saccharin						
Leucine						

[a]Estimated EC_{50} values were above the highest tested concentration.
[b]No fit for the 4-parametric curve, but some observed effects.
[c]Blank boxes correspond to no observed effects.

morphological neurite outgrowth assay for evaluation of neurotoxicity. Inhibition of neurite outgrowth is recognized as a neurotoxic event in humans and rodents, as well as *in vitro* (Krug *et al.*, 2013). Among the compounds were methyl mercury, rotenone, selected neurotoxic pesticides, flame retardants, and PAHs. Because toxic effects usually increase with prolonged exposure, we tested the effects of compounds using 3 different exposure times (1 h, 24 h, and 72 h) with independent plates for each time-point. Concentration-response effects of compounds were determined in a range of concentrations from 0.03 to 100 μM.

Most of the tested compounds perturbed the patterns of calcium oscillations (Figure 5), whereas the negative controls, saccharin and leucine, demonstrated no adverse effect (not shown). Most of the compounds that inhibited the frequency of spontaneous oscillations also decreased the peak amplitude and increased distance between peaks, whereas some compounds completely suppressed the spontaneous oscillations at higher concentrations. A few compounds, including 1-ethyl-3-methylimidazolium diethylphosphate, benzopyrene, and dibenz(a,c)anthracene increased peak count only at high concentrations. EC_{50} values for compound effects were calculated using peak count as readout (Table 2). Fourteen of the 22 tested compounds demonstrated effect at all 3 time-points, whereas several other compounds appeared to have an effect only after 24 h or 72 h. For some compounds, determination of EC_{50} values was complicated by non-monotonous concentration-dependency

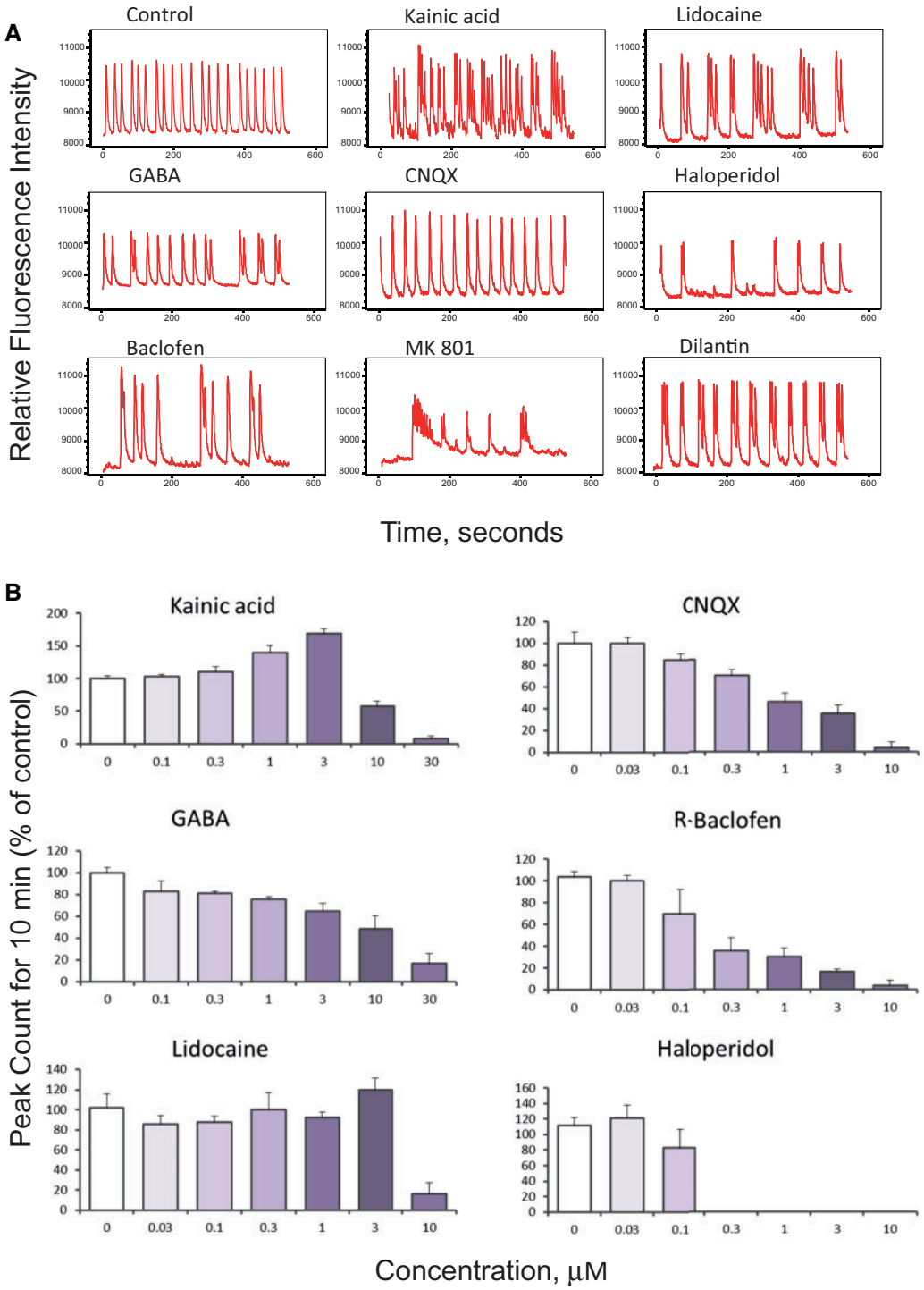

Figure 4. (A) Representative spontaneous calcium oscillation signal traces shown for selected modulators of neuronal activity. Graphs display phenotypic responses of neuronal activity after exposure to neuromodulators. Unaffected regular Ca^{2+} oscillations patterns are presented as a control (DMSO, 0.15%). Traces are shown for 1 μM concentrations for all compounds with exception of haloperidol (0.1 μM) and dilantin (10 μM). (B) Neural spheroids respond to glutamate agonist and antagonist (kainic acid and CNQX, respectively); both show concentration-dependent responses according to the expected mechanism of action of the compound on the excitatory system. Kainic acid induces an excitotoxicity response at concentrations greater than 3 μM. (C) Three-dimensional neural cultures respond to the GABAergic agonists GABA and baclofen, with reduced peak count. (D) The anesthetic lidocaine (voltage-gated sodium channel blocker) and the antipsychotic medication haloperidol (dopamine D_2 receptor antagonist) show modulatory effects. Peak counts were measured 60 min after compound addition. Data represent averages of $n = 3$ replicates with standard deviation bars (haloperidol $n = 2$, kainic acid $n = 4$). Highest concentrations for some compounds not shown at the bar graphs (because peak count =0).

responses or by lack of complete inhibition at the highest doses tested. Longer times of exposure resulted in a trend toward smaller EC_{50} values (Table 2), although several compounds had similar EC_{50} values across different exposure times. Based on this information we selected 24 h exposure time for screening the compound library.

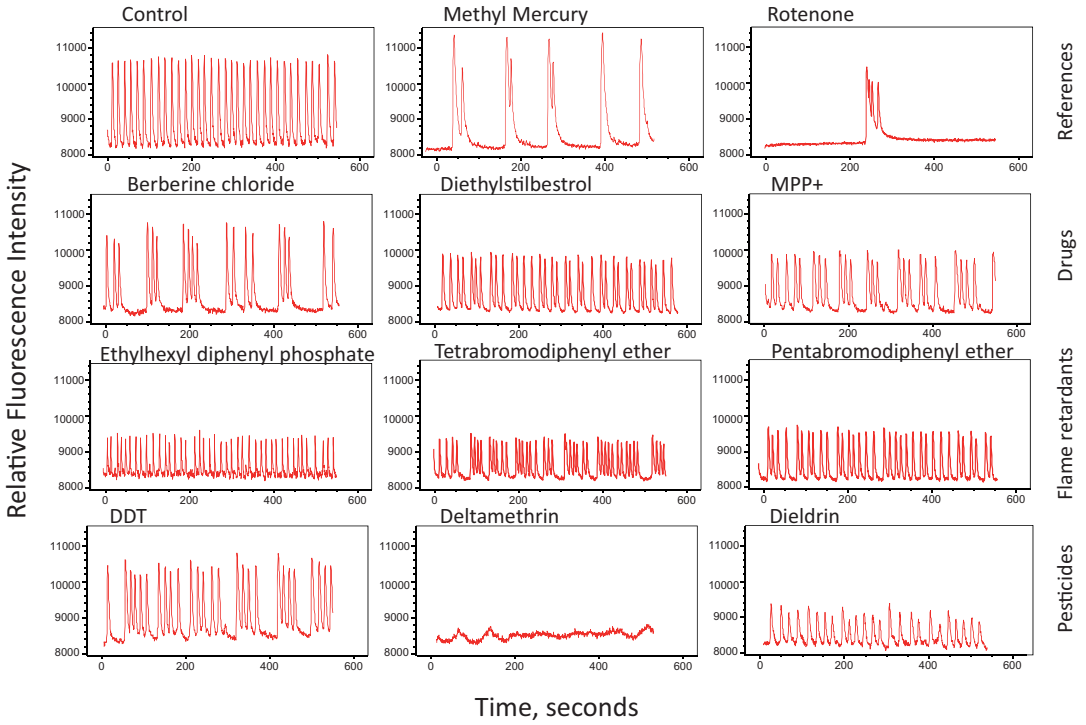

Figure 5. Representative calcium oscillation signal traces for neurotoxic compounds representing different chemical classes: pesticides, flame retardants, and drugs. Shown are typical phenotypic responses including unaffected regular Ca^{2+} oscillations patterns (DMSO). Traces are shown for effective concentrations of compounds: 0.3 μM for rotenone; 1 μM for DDT and deltamethrin, 3 μM for diethylstilbestrol, and 10 μM for other compounds.

Cellular and Mitochondrial Toxicity

Imaging methods were used to evaluate cell viability and mitochondria integrity to differentiate neuro-specific effects from general toxicity. Three-dimensional neural cultures were stained with viability dyes Calcein AM and MitoTracker Orange and nuclear dye Hoechst and imaged as described in the Materials and Methods section (Figure 6). Following image capture of 3D neural cultures, automated image analysis was performed for counting and characterization of cells in projection images (Supplementary Figs. 4 and 5). Compounds were tested over a concentration series ranging from 0.03 to 300 μM, for 3 different time points. Notably, none of the compounds from the list of neuroactive compounds (Table 1) showed significantly affected cell viability or mitochondria integrity after a 1 h exposure (data not shown). From the list of selected neurotoxic compounds only dieldrin and 2,2′,4,4′,5-pentabromodiphenyl ether (BDE-99) demonstrated a toxicity effect after 1 h of exposure. After 24 h and 72 h exposures, additional compounds, including berberine chloride, dieldrin, valinomycin, triphenyl phosphate, rotenone, methyl mercury, and lead, inhibited cell viability, as reflected by decreases in the appropriate cell numbers as compared with control samples (Figure 6, Table 2). The determination of EC_{50} values for viability markers was complicated due to the fact that most of the cytotoxicity effects were only observed at the highest concentration, 100 μM. Notably, EC_{50} values for the functional effects of most compounds, except lead, were having EC_{50} <10× lower than the estimated EC_{50} values for cytotoxicity.

Assay Variability

Another aspect of assay optimization is the evaluation of variability among endpoints related to calcium oscillations. As such, variability was assessed for different endpoints on inter- and intra-plate bases. We determined coefficients of variation (%CV) for control samples for each of the eight measurements (Figure 7) across 3 experiments. Overall, %CV values were lower than 20% for most measurements, with only one phenotype, peak rise time, exhibiting higher levels of variability (35.6%; Figure 7A). Coefficients of variance measured for various experiments are presented in Figure 7B and Supplementary Figure 6A. Inter-plate replicability was evaluated using quantitative comparison of data from different plates. Furthermore, the calculated concentration-responses for peak counts for 8 of the tested compounds were similar for 2 different plates (Figure 7C). The Pearson correlation coefficients comparing intra-plate data ranged from 0.71 for viability to 0.9 and 0.93 for peak count and peak amplitude, respectively. The Pearson correlation coefficients comparing inter-plate data ranged from 0.71 for peak rise to 0.84 and 0.86 for peak count and amplitude, respectively (Supplementary Figure 6B). In all cases, the correlation was significant ($p < .0001$).

Screening Chemical Library

As a next step, we used the method described above to evaluate a larger set of chemicals. The diversity of the chemical library was evaluated previously using principal component analysis based on 153 selected *in silico*-derived physicochemical descriptors (Sirenko *et al.*, 2017). Effects of compounds on peak count, width, and spacing, as well as average peak rise and decay times were determined in concentration-response using a range from 0.3 to 100 μM, with a few exceptions due to solubility. Chemicals were screened as duplicates after 24 h of compound exposure (Figure 8). Twenty-four control wells were used per plate to estimate the variance for vehicle-only treated cells. Vehicle controls did not differ significantly from untreated, media-only wells. Two independent experiments were

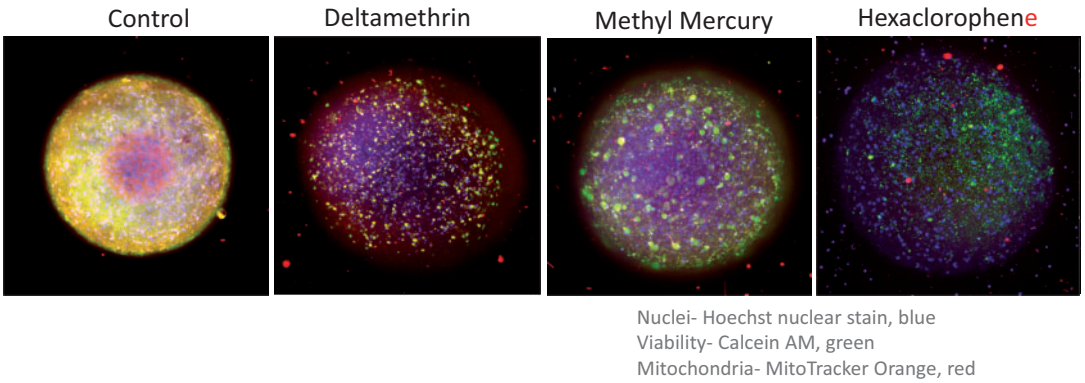

Figure 6. Composite projection images of 3D neural cultures treated with 30 μM of indicated compounds for 24 h and then stained with a nuclear stain (Hoechst 33342), viability stain (Calcein AM), and mitochondria potential dye MitoTracker Orange CMTMRos for 2 h (2 μM, 1 μM, and 0.5 μM, respectively). Spheroids were imaged with the DAPI, FITC, and TRITC, 10× Plan Fluor objective, imaged using Z-stack of confocal images (30 images, 15 μm apart). Maximum projection images were analyzed using custom module editor for detection of spheroid size and shape, and also count of positive and negative cells in each tissue. The images show nuclei (blue), Calcein AM stain (green), and mitochondria (red).

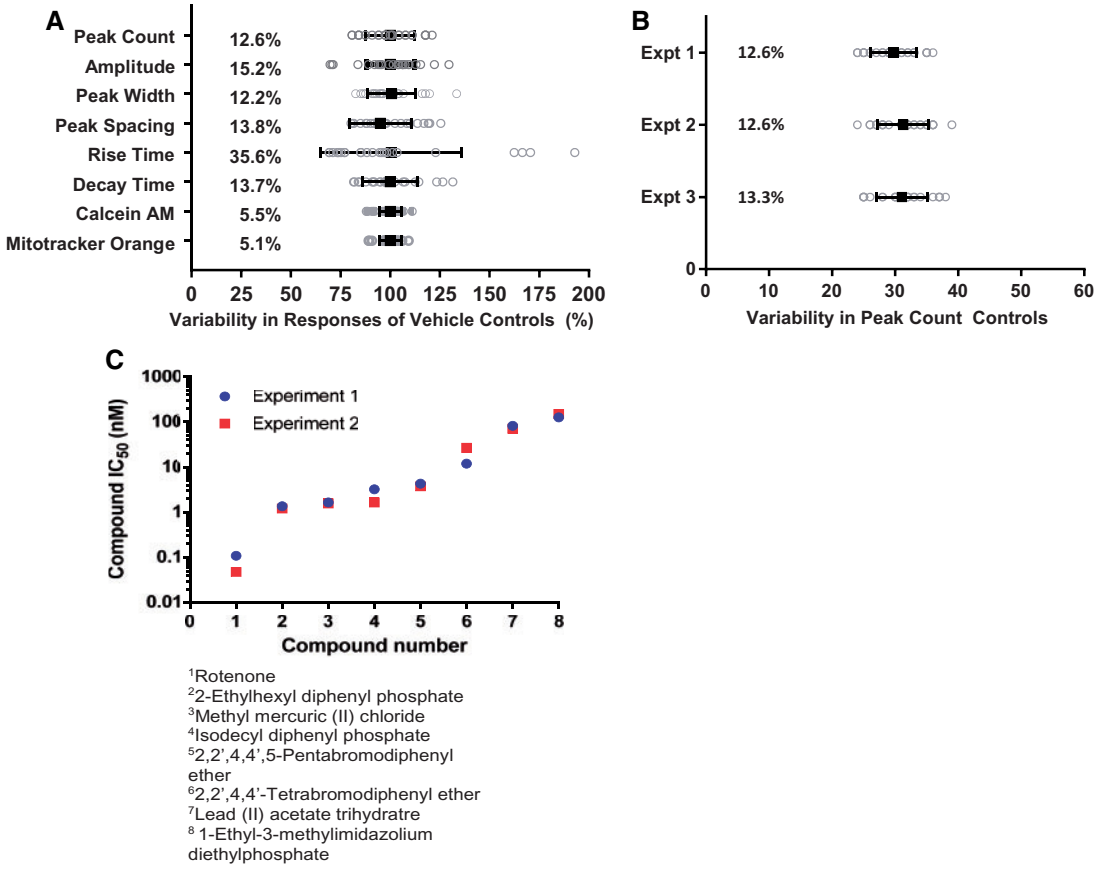

Figure 7. Assay variability for calcium oscillation and viability readouts. (A) Intra-plate variability of different measurements for the vehicle control samples within a representative plate, (DMSO) $n = 24$ after 24 h of incubation, data not normalized. Mean (black squares) is shown for each phenotype overlaid on top of gray circles representing individual well responses. Coefficients of variation (%CV) are shown for each phenotype. (B) Variabilities in vehicle controls for peak counts (per 10 min recording) measured for 3 representative plates. Mean is shown (black squares) for each of three experiments overlaid on top of gray circles representing individual well responses. %CVs are also shown for each experiment. (C) Comparison of compound responses (EC_{50} values) between 2 plates for 8 test compounds (24 h treatment). Pearson correlation between experiments was $r = 0.987$ $p < .0001$, Spearman correlation $r = 1.000$, $p < .0001$.

performed on different days using the same protocol, reagents, and instruments but with different lots of 3D neural cultures as well as different sets of compound dilutions. A subset of normalized data for peak count and viability measurements is presented in Figure 8. The oscillatory behavior of the 3D neural cultures exposed to compounds was segregated according to the sub-categories for drugs, pesticides, flame retardants, polyaromatic hydrocarbons, and the group of compounds labeled as industrial, which includes metals and additional chemicals. The full data set for the different readouts, raw data and normalized data, are included in Supplementary Table 2. Importantly, peak counts and viabilities as well as other

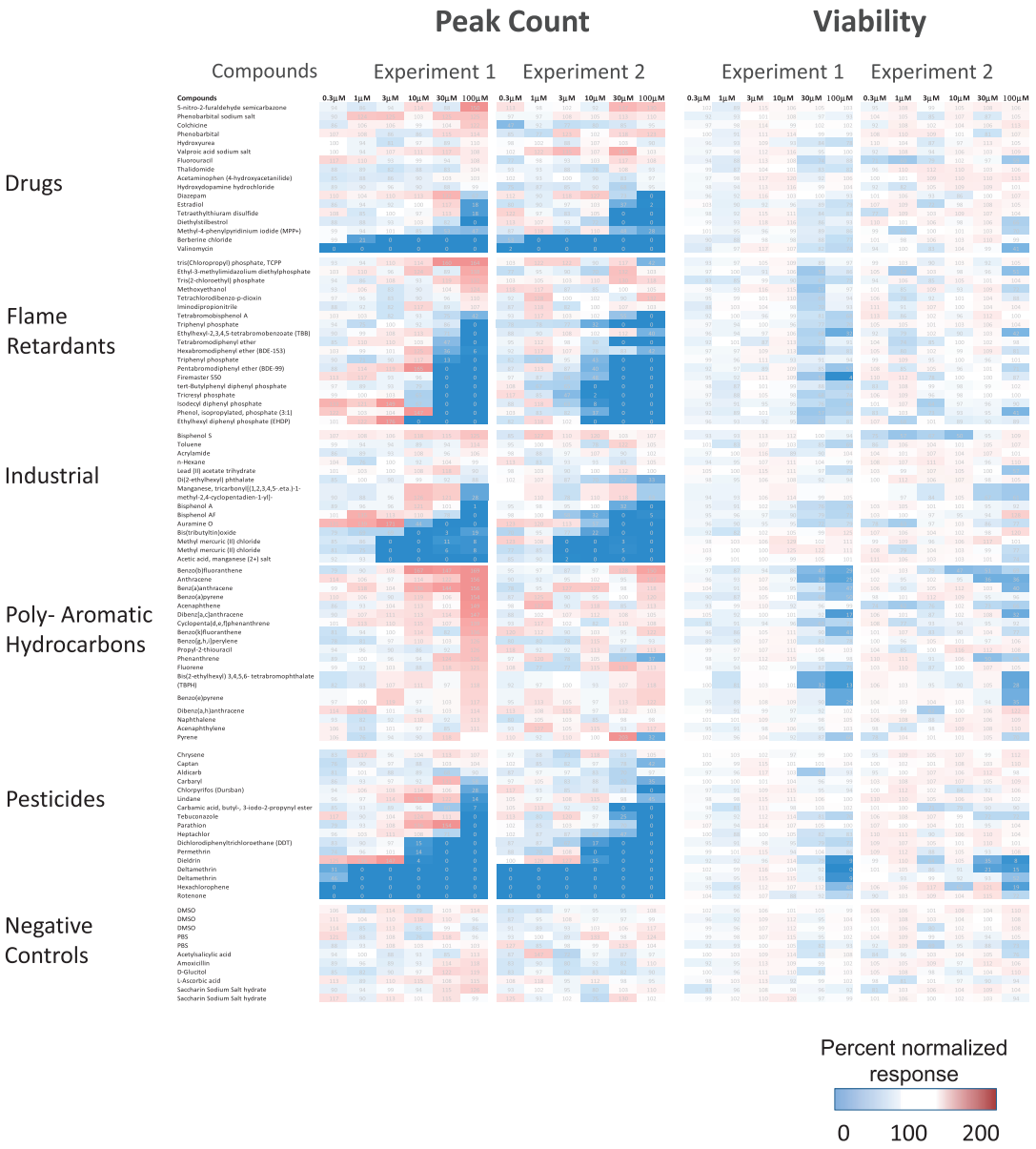

Figure 8. Heat map showing quantitative normalized concentration-response data for two selected measurements: the calcium oscillation peak counts (per 10 min) and cell viability for concentration range of 0.3–100 μM after 24 h of treatment. Responses at each time point and concentration are shown as a heat map (scale bar legend is on a side of the figure).

readouts exhibited considerable concordance between the experiments, both without treatment and upon exposure to compounds (Figure 8, Supplementary Table 2). There was a significant correlation in the measured values, patterns of compound effects, and concentration-responses. Forty-seven compounds demonstrated responses that were 3 standard deviations or more from the averaged measurements from control wells in two-independent experiments. Five compounds (PAHs) also had responses greater than 3 standard deviations from control but only in the first experiment.

Comparative analysis of normalized concentration-response data revealed that the negative controls saccharin, acetaminophen, and acetic acid did not result in alterations of intracellular Ca^{2+} oscillations. However, many of the tested chemicals affected the pattern of calcium oscillations in a concentration-dependent manner (Figure 8). The positive controls methyl mercury, rotenone and valinomycin strongly inhibited calcium oscillations at the lowest doses (0.3–1 μM). Also, the pesticides dichlorodiphenyltrichloroethane (DDT), deltamethrin, dieldrin, and permethrin exhibited strong negative chronotropic effects at concentrations from 3 to 10 μM. Other pesticides including heptachlor and carbamic acid were capable of affecting oscillation patterns at higher concentrations (100 μM). Flame retardants, including triphenyl phosphate, phenol isopropylated phosphate (3:1), 2-ethylhexyl diphenyl phosphate, 2,2′,4,4′,5-pentabromodiphenyl ether, and 2,2′,4,4′-tetrabromodiphenyl ether, represented another group of chemicals with pronounced physiologic effects at concentrations exceeding 10 μM. Interestingly, for some compounds, peak count increase was observed along with decreased amplitude, preceding the decrease in peak rate or stopping oscillations. Several PAHs including acenaphthene, acenaphthylene, 4-H-cyclopenta (d,e,f)phenanthrene, fluorene, pyrene, anthracene, benz(a)-anthrancene, benzo(e)pyrene, benzo(k)fluoranthene, and

benzo(b)fluoranthene moderately increased the peak frequency, with a stronger effect seen in Experiment 1. This group demonstrated the most discrepancies between the two experiments, whereas effects of other compounds were consistent between both experiments. Some drugs and substances including berberine chloride, 1-methyl-4-phenypyridinium (MPP+), and diazepam had significant effects on oscillation patterns, as did the hexachlorophene and several bisphenols.

A number of the tested chemicals exhibited a hormesis-like concentration-response pattern with initial increases in the oscillation peak frequency followed by a sudden inhibition of calcium oscillations. Examples include the pesticides parathion, phenol isopropylated phosphate (3:1), auramine O, 2-ethylhexyl diphenyl phosphate (EHDP), and 2,2′,4,4′,5-pentabromodiphenyl ether.

We noted that only a few tested compounds had effects on cell viability or mitochondria integrity after 24 h. Those include 2-ethylhexyl-2,3,4,5-tetrabromobenzoate, 2,2′,4,4′,5-pentabromodiphenyl ether, bis(2-ethylhexyl) 3,4,5,6-tetrabromophthalate, dieldrin, hexachlorophene, rotenone, valinomycin, and deltamethrin, as well as the group of PAHs. For these chemicals, decreases in peak frequencies occurred at lower concentrations than reduced cell viability indicating that modulation of calcium oscillation may be a more sensitive indicator of neuronal toxicity.

A number of tested compounds in this library did not elicit significant effects on intracellular Ca^{2+} oscillations at the tested concentrations. These included mostly drugs (ie, phenobarbital, 5-fluorouracil, acetylsalicylic acid, valproic acid, and thalidomide) and also some PAHs (eg, naphthalene, benzo(e)pyrene, and benzo[g,h,i]perylene), pesticides (eg, aldicarb, captan, and chrysene), and a flame retardant (tris(2-chloroethyl) phosphate), as well as acrylamide, colchicine, and several other compounds.

Analysis of the Concentration-Responses

For the screening library, concentration-responses data were analyzed using the BMCs instead of the EC_{50} values (see the Materials and Methods section). Concentration-response data were fit to a four-parameter maximum-likelihood Hill model as described previously in Reif *et al.* (2013), Ryan *et al.* (2016), Sirenko *et al.* (2017), and Wignall *et al.* (2014). In accordance with the US EPA guidance for dose-response modeling (EPA, 2012) and determination of POD values, we selected a three standard deviation departure from the control mean as the BMC from which a POD was derived. If the maximum response did not reach this level in the concentration range tested, the 'no observable adverse effect level' was recorded as 100 μM, reflecting the highest concentration used in the respective assay. If the effect was observed at lowest dose tested, the lowest dose tested (0.3 μM) was considered as POD (or BMC—benchmark concentration). Identical curve fitting and BMC derivation procedures were applied to all chemicals and phenotypes collected. Figure 9A presents ranking of chemicals according for their toxic effects, using peak count for ranking determination. The peak count was chosen for compound ranking because of its lowest variability, highest reproducibility, and ease of visualization. The BMC values for other readouts are also presented in the same figure. The numeric data are presented in Supplementary Table 3.

BMC Values and Compound Selectivity

To determine whether the observed physiologic effects were findings related to neurotoxicity or due to non-specific cytotoxicity, we quantified the degree of specificity to parameter changes using a calculated selectivity score (SS). This score is defined as the ratio between a POD for a specific neurophysiologic phenotype, such as peak count, and the associated cell viability (ie, $POD_{cell\ viability}/POD_{Ca2+\text{-}oscillation\ readout}$). An increased SS is equivalent to increased neurotoxic specificity. Herein, we defined a compound as 'selective' if there was at least one log10 or greater (~3 fold) difference between neurophysiologic and cytotoxic responses ($SS \geq 3$), which corresponds to a difference of at least one compound dilution step. The estimated POD (BMC—benchmark concentration) values and calculated ratios for each compound are summarized in Supplementary Table 3. In cases when a BMC for viability could not be computed because the viability response was less than 3 standard deviations from the control, a nominal BMC of 100 μM was used as the viability BMC in the selectivity calculation.

In total, 47 of the 82 tested chemicals (57%, excluding negative controls that showed no effect) were associated with $POD_{Ca^{2+}\ oscillation}$ values lower than 100 μM after 24 h of exposure. Considering the low observed cytotoxicity at this point (only few chemicals with an associated $POD_{cell\ viability}$ below 30 μM), 27 of these compounds fulfilled the above defined criteria for neurotoxic selectivity. Figure 9B illustrates the list and ranking for 'selective' neurotoxic compounds by lowest BMC. BMCs as well as selectivity scores are presented in Supplementary Table 3.

Variability of Screening Data

In addition to the qualitative comparison, assay variability was assessed for different measurements on inter- and intra-plate bases. The inter-plate replicability was evaluated using quantitative comparison of data from two-independent experiments. Correlation analysis for inter-plate raw values for peak count, amplitude, and viability (Calcein AM) revealed Pearson *r* values of 0.9, 0.9, and 0.84, respectively (Supplementary Figure 7), whereas for other readouts (peak rise, decay times, spacing) the correlation coefficients were lower (>0.5), reflecting the increased complexity and higher variability of those readouts. A similar trend was observed for Spearman coefficients (values ranged from 0.88, 0.91 for peak count and amplitude to 0.68 for spacing). When comparing the data across 2 experiments, despite the fact that experiments were performed using different batches of 3D neural culture 384-well plates, correlation analysis for inter-plate normalized values for peak count, amplitude, and peak width revealed high Pearson correlation *r* values of 0.92, 0.93, and 0.77, respectively (Supplementary Figs. 7 and 8). For other readouts (peak rise, decay times, spacing) the correlation coefficients were <0.5, with the lowest value for peak decay times. For Spearman coefficients, values were relatively higher and ranged from 0.87 and 0.89 for peak count and amplitude, respectively, to 0.6 for peak spacing (Supplementary Figure 8).

DISCUSSION

Development of novel *in vitro* approaches for rapid toxicity testing and dose-response analysis of chemicals is an active area of investigation (Judson *et al.*, 2009a,b; Tice *et al.*, 2013). Human iPSC-derived cell types, including neurons, have become increasingly attractive as *in vitro* systems for both toxicity evaluation and mechanistic studies due to their physiological relevance in comparison to transformed cell lines and greater supply as compared with primary cells (Acimovic *et al.*, 2014; Verstraelen *et al.*, 2014; Anson *et al.*, 2011; Mordwinkin *et al.*, 2013; Sinnecker *et al.*, 2014; Suter-Dick *et al.*, 2015). Furthermore, combining iPSC-derived human cell types with 3D culture formats has the potential to generate even more relevant model systems for analyzing the pathogenesis and progression of diseases, evaluating drug treatments, and advancing the

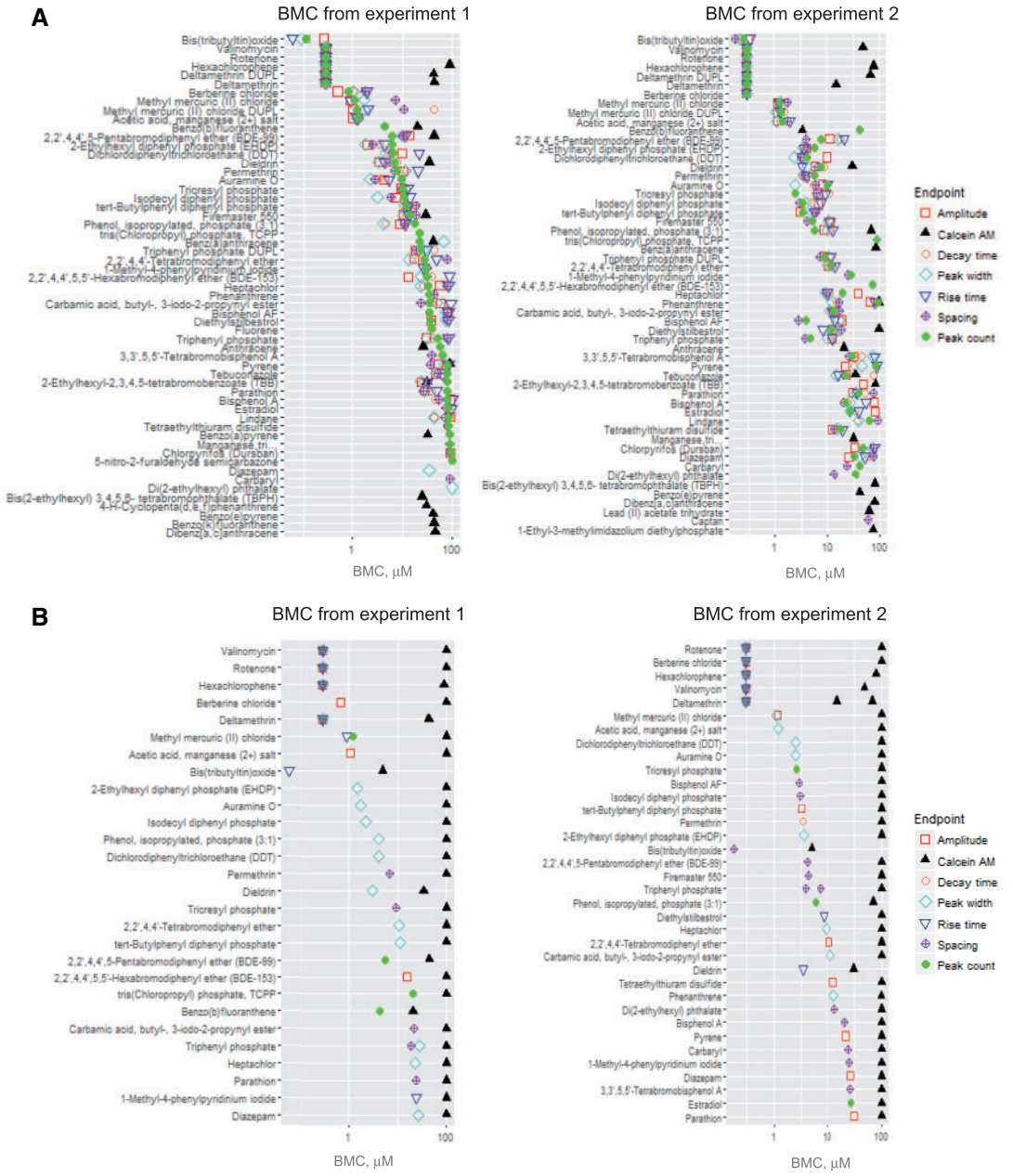

Figure 9. (A) Compounds ranked according to the Bench Mark Concentrations (BMC) for peak count (per 10 min recording) values. Values for other calcium readout measurements are shown as different symbols. (B) Compounds were ranked according to their selectivity. Selectivity defined as > the square root of 10 (a difference of >0.5 in the $\log_{10}$ of the BMC), based on the ratios between the lowest non-viability BMC (calcium oscillation read-outs) and BMC for viability (Calcein AM assay).

understanding of complexity of tissue biology (Khademhosseini *et al.*, 2006; Kunz-Schughart *et al.*, 2004; Langer and Tirrell, 2004 Kijanska, and Kelm, 2004). 3D cultures are believed to have the advantage of closely recapitulating important attributes of tissues including architecture, cell organization, cell-cell and cell-matrix interactions, and more physiologically relevant diffusion characteristics. Several studies have indicated the presence of a more mature phenotype on 3D versus 2D cultures including cell morphology, neuronal activity, pharmacological responses, and gene expression profiles specific for maturity (Camp *et al.*, 2015; Luo *et al.*, 2016; Renner *et al.*, 2017). Importantly, the significant advantage of the 3D system used in this study was the highly homogenous calcium signal achieved across the plate and between different plates and batches. We hypothesized that the confined 3D space may provide a more homogenous differentiation environment reducing the variability commonly observed with iPSC-derived neural 2D cultures (data not shown).

Under normal physiologic conditions, calcium signaling within the brain affects intracellular function, action potentials (ie, neuronal activity), and communication between cells (ie, neurons and astrocytes). Dysregulation of calcium signaling could have deleterious consequences leading to necrosis or disease progression and has been indicated as one of the early-stage processes in the pathogenesis of neurodegenerative diseases (Bezprozvanny, 2010; Magi *et al.*, 2016). Although intracellular calcium levels in the nervous system are difficult to

monitor in animal models, newer *in vitro* platforms are emerging that may be able to detect chemical-mediated effects of calcium regulation in real time (Duff Davis and Schmidt, 2000).

In this study, we characterized kinetic and confocal imaging methods that are compatible with automated instruments and demonstrated the potential utility of human iPSC-derived 3D neural spheroid cultures for toxicity screening. We focused on optimizing an intracellular Ca^{2+} oscillation assay in 3D neural cultures and on generating high-resolution imaging methods that allow for the characterization of morphological changes. Also, we showed that multi-parameter functional and morphological analysis of calcium oscillations delivers informative readouts that enable screening for deleterious effects of test compounds on neuronal function. However, the biological effects maybe more complex, because calcium is also known to promote plasticity and adaptive changes (Clemens and Johnston, 2014). Finally, we showed that cell morphology and viability can also be used as a screening assay in these cultures to interrogate neurotoxicity (Beattie *et al.*, 2000; Carroll *et al.*, 2001; Choi *et al.*, 1988). It should be noted that, whereas we propose a workflow for the assays, alternative instruments and reagents can potentially be used for recording and analysis of calcium oscillations, viability assessment, or high content imaging (eg, FDSS, Hamamatsu, Japan; Opera Phenix, PerkinElmer, MA; FlexStation 3, Molecular Devices), but the methods may need to be adjusted for other platforms.

Whereas detailed characterization of responses to various agonists and antagonists was out of the scope of this study, here, we demonstrated sensitivity of the assay to neuroactive substances and known neurotoxic compounds. Furthermore, a time-course for toxicity effects was evaluated with a selected set of known neurotoxic compounds. Effects on calcium oscillations increased with time for many compounds, which is consistent with the assumption that longer exposures may cause greater toxicity effects.

Following assay characterization, we screened a library of 87 chemicals that included four major chemical classes with agents of known or suspected neurotoxic potential, including pesticides (Dingemans *et al.*, 2011; Gao *et al.*, 2002; Hassenklöver *et al.*, 2006; Abou-Donia 2003; Hendriks and Westerink, 2015; Jang *et al.*, 2015; Ryan *et al.*, 2016; Tang *et al.*, 2003), flame retardants (Flaskos, 2012; Hassenklöver *et al.*, 2006; Lema *et al.*, 2007), PAHs (Billiard *et al.*, 2006; Burstyn *et al.*, 2005), and drugs (Li *et al.*, 2001) as well as compounds with unknown neurotoxic potential, and 5 negative controls. More than half of the tested compounds, 47 out of 82 (57%, excluding controls), demonstrated concentration-dependent perturbation of the calcium oscillation patterns, which we propose as a screening phenotype for neurotoxicity (Figure 10). Among those, 14 (out of 16) that tested positive were pesticides, and 14 (out of 19) were flame retardants. Notably, out of the 82 compounds 38 have previously been classified as DNT/NT by other assays in the literature (Behl *et al.*, in preparation), and of those 38, 24 compounds tested positive in the assay. Most of the known neurotoxic pesticides were active in the assay (12 out of 14). The known neurotoxic mechanisms of action for pesticides include acetylcholinesterase inhibitors (eg, organophosphate or carbamate insecticides), sodium channel modulators (eg, Type I and II pyrethroids), chloride channel modulators (organochlorine insecticides), or redox cyclers (eg, bipyridyl herbicides) whereas some classes have uncharacterized mechanisms (Bjørling-Poulsen *et al.*, 2008; Deshpande *et al.*, 2016). Even though calcium is not typically a direct target of most pesticides, its dysregulation following exposure has been reported with organophosphates such as

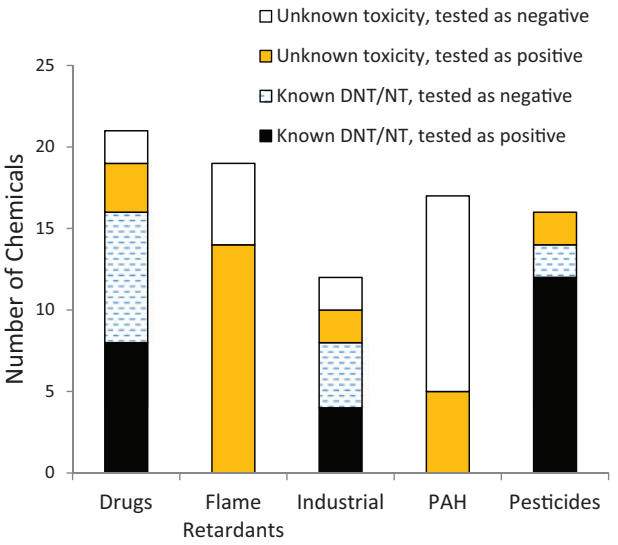

Figure 10. Numbers of compounds from different categories tested positive or negative in the assay. The x-axis shows categories of compounds, and the y-axis shows the total number of compounds tested as positive/negative in the assay. The black bar indicates compounds that have previously been classified as developmental neurotoxicants (DNT) or neurotoxicants (NT) in the literature that were active (positive) in this assay; the dashed bar shows compounds that are classified as DNT/NT compounds in the literature that tested negative in this assay; the orange bar (the gray in back-white version) shows compounds with unknown toxicities that were positive and the white bar shows compounds with unknown toxicity in the literature which were tested as negative in the assay.

chlorpyrifos (Meijer *et al.*, 2015), organochlorines such as lindane and dieldrin (Hendriks and Westerink 2015; Heusinkveld *et al.*, 2010), or pyrethroids such as deltamethrin (Bjørling-Poulsen *et al.*, 2008), which were examined in this study. Only half of the drugs that have been reported as known neurotoxicants tested as positive in this assay. Some of the reasons might be the lack of proper metabolism (6-propyl-2-thiouracil), a mechanism of action that includes cell proliferation (5-FU, colchicine, hydroxyurea), or the need for longer exposure. There were marginal effects of lead, hexane, toluene, chlorpyrifos, and thalidomide that were not statistically significant. The marginal effects of toluene and hexane may be partially explained by volatility concerns associated with these compounds. Thalidomide is also better known as a developmental toxicant although DNT effects have been noted (Qin *et al.*, 2012; Vorhees *et al.*, 2001). However, because mechanistically, thalidomide is known to affect embryogenesis at a critical stage of development, mainly through angiogenesis (Vargesson, 2015), it is not surprising that its effects are not captured in this assay.

Our results are generally concordant with reports describing the neurotoxicity potential for a number of compounds (eg, berberine chloride [Yan *et al.*, 2015], valinomycin [Vogel and Sperelakis, 1978], tetraethylthiuram disulfide [Lee and Peters, 1976; Travis *et al.*, 2014], diethylstilbestrol [Martinez *et al.*, 2001]). In addition, compounds with unknown neurotoxic potential including 14 of the 19 flame retardants were captured by this assay (Figure 10). Flame retardants are used worldwide, and many have been postulated to be neurotoxic through varied mechanisms. Organophosphate flame retardants such as triphenyl phosphate are suggested cause neurotoxicity similar to other acetylcholinesterase inhibitors (Behl *et al.*, 2016), although reports suggest that these compounds can also alter intracellular calcium (Abou-Donia, 2003). Brominated flame retardants

including tetrabromobisphenol-A have been reported to cause toxicity through multiple mechanisms including inhibition of voltage-gated calcium channels (Hendriks *et al.*, 2012). Results from this assay, coupled with recent preliminary evidence suggesting that these compounds demonstrate neurotoxicity *in vitro* and in alternate models (Behl *et al.*, 2016; Dishaw *et al.*, 2014; Jarema *et al.*, 2015), point towards the need for further in-depth hazard characterization of these compounds.

Whereas the mechanisms of action for the effects of some compounds are known, eg inhibition of GABA and AMPA receptors or ion channels resulting in inhibition of neuronal activation (Bloomquist, 1996; Casida, 1993; Ffrench-Constant *et al.*, 2016), for most environmental chemicals, the mechanisms are unknown or not clearly defined. These mechanisms may include effects on ion channels (Narahashi, 1996), the $GABA_A$ receptor chloride channel complex (Ogata *et al.*, 1988), and voltage-dependent Ca^{2+} currents (Hassenklöver *et al.*, 2006). Although a thorough mechanistic evaluation of the chemicals included in the screening library was not within the scope of this study, it would be reasonable to hypothesize that interference with ion channels may at least partially contribute to the increase or decrease in the peak frequency observed in the Ca^{2+} oscillation measurements.

In contrast to the functional Ca^{2+} oscillation results in which compound effects were readily detected, the high content imaging-based morphology/cell viability assay detected a substantial loss of cell viability only for a subset of compounds (19 of the 87) that were tested after exposure for 24 h of treatment. This observation indicates that changes in Ca^{2+} oscillations can be evaluated as a specific effect related to neurotoxicity compared with non-specific effects on cell viability that occur later.

A limitation of the assay approach for evaluation of neurotoxicity is similar to most *in vitro* assays in that there is a lack of organ-like metabolism. However, the developing ability to link organ-specific systems together makes it likely that this limitation will be overcome in the near future. Another limitation is the fact that Ca^{2+} oscillation is not a direct measure for neuronal electrophysiology. Nonetheless, our data demonstrate its value as a functional screening assay for potential chemical-mediated neurotoxic effects. In addition, iPSC-derived cells resemble fetal rather than adult neurons, however this fact potentially can be considered for evaluation of developmental neurotoxicity (Luo *et al.*, 2016). Another limitation of this work is that *In vitro* models in general, as well as one presented herein, are not able to replicate the complete array of the types of neurotoxicity that can be detected *in vivo*. Whereas the effects of the test compounds on calcium flux that we observed can be interpreted relative to general cytotoxicity, as recommended by Judson *et al.* (2009b), this model would not likely detect effects on axon myelination, effects on neuroglia, mechanisms of synaptic transmission of neurotransmitters, and other important effects that may result in neurotoxicity. Despite these limitations, currently available iPSC-derived neurons have clearly proven their utility and in predicting chemical-induced neuronal functional and toxicity phenotypes and are widely accepted as useful screening tools (Acimovic *et al.*, 2014; Anson *et al.*, 2011; Choi *et al.*, 2014; Jorfi *et al.*, 2018).

To our knowledge, this is the first study to characterize calcium oscillations in a spontaneous, synchronized 3D human iPSC-based high-throughput organotypic model as a screening tool for neurotoxicity. It is a comprehensive evaluation of a diverse set of environmental toxicants in a novel human neural 3D culture model that not only has utility for neurotoxicity screening but also potentially for drug safety evaluation. Neurotoxicity testing is an unmet need in the current screening program of environmental chemicals, and this study demonstrates that 3D neural co-culture platforms are a robust, reproducible, and informative high-throughput platform that can be incorporated into the Tox21 program (https://ntp.niehs.nih.gov/results/tox21/researchphases/index.html) or other similar efforts. We demonstrate that the multiplexing of several independent read-outs enables selectivity of the effects with respect to neuronal function. Finally, the multiplexed analysis and concentration-response profiling allows for ranking of compounds and the ultimate use of these data in risk-based evaluations by comparing the *in vitro* effects of chemicals with human exposure levels (Wambaugh *et al.*, 2015) as well as for prioritization for further *in vitro* and *in vivo* toxicology studies. Some future studies include comparing the sensitivity of calcium signaling in this model with other non-neural models to address specificity to the nervous system. Whereas we recognize that calcium signaling is only one aspect of capturing effects related to neurotoxicity, we envision that this model, combined with other screening assays (Behl *et al.*, in preparation; Harrill *et al.*, 2013) could serve as a powerful path forward to identify environmental compounds with unknown neurotoxic potential.

SUPPLEMENTARY DATA

Supplementary data are available at *Toxicological Sciences* online.

ACKNOWLEDGMENTS

The authors would like to acknowledge technical support and useful discussions with Matthew Hammer, as well as the useful comments from Peter Miu, Ivan Rusyn, and Jeff Weber. The authors would also like to thank Dr Johanna Nyffeler, USEPA for her valuable review.

DISCLOSURES

Oksana Sirenko, Carole Crittenden, and Grischa Chandy are employed by Molecular Devices LLC, which sells the ImageXpress Micro systems, MetaXpress software, FLIPR Tetra system, and FLIPR Calcium 6 Assay Kit. Cassiano Carromeu, Steven Dea, Steven Biesmans, Neha Sodhi, Sergio Mora, Oivin Guicherit, Ryan Gordon, and Fabian Zanella are employed by StemoniX, Inc that provided the iPSC-derived cell models. The views expressed in this paper are those of the authors and do not necessarily reflect the views or policies of the National Institutes of Health. Mention of trade names or commercial products does not constitute endorsement or recommendation for use.

FUNDING

This work was supported by internal funding from Molecular Devices, LLC, StemoniX Co, and National Institute of Environmental Health Sciences.

REFERENCES

Abou-Donia, M. B. (2003). Organophosphorus ester-induced chronic neurotoxicity. *Arche. Environ. Health* **58**, 484–497.

Acimovic, I., Vilotic, A., Pesl, M., Lacampagne, A., Dvorak, P., Rotrekl, V., and Meli, A. C. (2014). Human pluripotent stem

cell-derived cardiomyocytes as research and therapeutic tools. *Biomed. Res. Int.* **2014**, 1.

Anson, B. D., Kolaja, K. L., and Kamp, T. J. (2011). Opportunities for use of human iPS cells in predictive toxicology. *Clin. Pharmacol. Ther.* **89**, 754–758.

Arvanov, V. L., Liang, X., Schwartz, J., Grossman, S., and Wang, R. Y. (1997). Clozapine and haloperidol modulate N-methyl-D-aspartate- and non-N-methyl-D-aspartate receptor-mediated neurotransmission in rat prefrontal cortical neurons *in vitro*. *J. Pharmacol. Exp. Ther.* **283**, 226–234.

Beattie, E. C., Carroll, R. C., Yu, X., Morishita, W., Yasuda, H., von Zastrow, M., and Malenka, R. C. (2000). Regulation of AMPA receptor endocytosis by a signaling mechanism shared with LTD. *Nat. Neurosci.* **3**, 1291–1300.

Behl, M., Rice, J. R., Smith, M. V., Co, C. A., Bridge, M. F., Hsieh, J. H., Freedman, J. H., and Boyd, W. A. (2016). Editor's highlight: Comparative toxicity of organophosphate flame retardants and polybrominated diphenyl ethers to *Caenorhabditis elegans*. *Toxicol. Sci.* **154**, 241–252.

Betts, K. S. (2013). Tox21 to date: Steps toward modernizing human hazard characterization. *Environ. Health Perspect.* **121**, A228.

Bezprozvanny, I. B. (2010). Calcium signaling and neurodegeneration. *Acta Nat.* **2**, 72–82.

Billiard, S. M., Timme-Laragy, A. R., Wassenberg, D. M., Cockman, C., and Giulio, R. T. (2006). The role of the aryl hydrocarbon receptor pathway in mediating synergistic developmental toxicity of polycyclic aromatic hydrocarbons to zebrafish. *Toxicol. Sci.* **92**, 526–536.

Bjørling-Poulsen, M., Andersen, H. R., and Grandjean, P. (2008). Potential developmental neurotoxicity of pesticides used in Europe. *Environ. Health* **7**, 50.

Bloomquist, J. R. (1996). Ion channels as targets for insecticides. *Annu. Rev. Entomol.* **41**, 163–190.

Burstyn, I., Kromhout, H., Partanen, T., Svane, O., Langard, S., Ahrens, W., Kauppinen, T., Stucker, I., Shaham, J., Heederik, D., *et al.* (2005). Polycyclic aromatic hydrocarbons and fatal ischemic heart disease. *Epidemiology* **16**, 744–750.

Caeser, M., Evans, M. L., and Benham, C. D. (1999). Lack of effect of the novel anticonvulsant SB-204269 on voltage-dependent currents in neurones cultured from rat hippocampus. *Neurosci. Lett.* **271**, 57–60.

Camp, J. G., Badsha, F., Florio, M., Kanton, S., Gerber, T., Wilsch-Bräuninger, L. E., Sykes, A., Hevers, W., , and Lancaster, M. (2015). Human cerebral organoids recapitulate gene expression programs of fetal neocortex development. *Proc. Natl. Acad. Sci. U.S.A.* **112**, 15672–15677.

Cao, Z., Hammock, B. D., McCoy, M., Rogawski, M. A., Lein, P. J., and Pessah, I. N. (2012). Tetramethylenedisulfotetramine alters Ca^{2+} dynamics in cultured hippocampal neurons: Mitigation by NMDA receptor blockade and GABA(A) receptor-positive modulation. *Toxicol. Sci.* **130**, 362–372.

Carroll, R. C., Beattie, E. C., von Zastrow, M., and Malenka, R. C. (2001). Role of AMPA receptor endocytosis in synaptic plasticity. *Nat. Rev. Neurosci.* **2**, 315–324.

Casida, J. E. (1993). Insecticide action at the GABA-gated chloride channel: Recognition, progress, and prospects. *Arch. Insect Biochem. Physiol.* **22**, 13–23.

Chang, T. T., and Hughes-Fulford, M. (2009). Monolayer and spheroid culture of human liver hepatocellular carcinoma cell line cells demonstrate distinct global gene expression patterns and functional phenotypes. *Tissue Eng. A* **15**, 559–567.

Choi, S. H., Kim, Y. H., Hebisch, M., Sliwinski, C., Lee, S., D'Avanzo, C., Chen, H., Hooli, B., Asselin, C., Muffat, J., *et al.* (2014). A three-dimensional human neural cell culture model of Alzheimer's disease. *Nature* **515**, 274–278.

Choi, D. W., Koh, J. Y., and Peters, S. (1988). Pharmacology of glutamate neurotoxicity in cortical cell culture: Attenuation by NMDA antagonists. *J. Neurosci.* **8**, 185–196.

Chou, M. Y., Lee, C. Y., Liou, H. H., and Pan, C. Y. (2014). Phenytoin attenuates the hyper-exciting neurotransmission in cultured embryonic cortical neurons. *Neuropharmacology* **83**, 54–61.

Clemens, A. M., and Johnston, D. (2014). Age- and location-dependent differences in store depletion-induced h-channel plasticit in hippocampal pyramidal neurons. *J. Neurophysiol.* **111**, 1369–1382.

Cohen, E., Ivenshitz, M., Amor-Baroukh, V., Greenberger, V., and Segal, M. (2008). Determinants of spontaneous activity in networks of cultured hippocampus. *Brain Res.* **1235**, 21–30.

Coyne, L., Su, J., Patten, D., and Halliwell, R. F. (2007). Characterization of the interaction between fenamates and hippocampal neuron GABA(A) receptors. *Neurochem. Int.* **51**, 440–446.

Crawford, M. L., and Young, J. M. (1988). GABAB receptor-mediated inhibition of histamine H1-receptor-induced inositol phosphate formation in slices of rat cerebral cortex. *J. Neurochem.* **51**, 1441–1447.

Derecki, N. C., Privman, E., and Kipnis, J. (2010). Rett syndrome and other autism spectrum disorders—Brain diseases of immune malfunction? *Mol. Psychiatry* **15**, 355–363.

Deshpande, L. S., Blair, R. E., Phillips, K. F., and DeLorenzo, R. J. (2016). Role of the calcium plateau in neuronal injury and behavioral morbidities following organophosphate intoxication. *Ann. N.Y. Acad. Sci.* **1374**, 176–183.

Dingemans, M. M., van den Berg, M., and Westerink, R. H. S. (2011). Neurotoxicity of brominated flame retardants: (In)direct effects of parent and hydroxylated polybrominated diphenyl ethers on the (developing) nervous system. *Environ. Health Perspect.* **119**, 900–907.

Dishaw, L.V., Hunter, D.L., Padnos, B., Padilla, S., Stapleton, H.M. (2014). Developmental exposure to organophosphate flame retardants elicits overt toxicity and alters behavior in early life stage zebrafish (Danio rerio). *Toxicol Sci.* **142**, 445–454.

Dravid, S. M., and Murray, T. F. (2004). Spontaneous synchronized calcium oscillations in neocortical neurons in the presence of physiological [Mg(2+)]: Involvement of AMPA/kainate and metabotropic glutamate receptors. *Brain Res.* **1006**, 8–17.

Duff Davis, M., and Schmidt, J. J. (2000). *In vivo* spectrometric calcium flux recordings of intrinsic Caudate-Putamen cells and transplanted IMR-32 neuroblastoma cells using miniature fiber optrodes in anesthetized and awake rats and monkeys. *J. Neurosci. Methods* **99**, 9–23.

EPA, U. (2012). *Benchmark Dose Technical Guidance*. US Environmental Protection Agency, Washington, DC.

Ffrench-Constant, R. H., Williamson, M. S., Davies, T. G. E., and Bass, C. (2016). Ion channels as insecticide targets. *J. Neurogenet.* **30**, 163–177.

Filer, D. L., Kothiya, P., Setzer, R. W., Judson, R. S., and Martin, M. T. (2017). The ToxCast pipeline for high-throughput screening data. *Bioinformatics* **33**, 618–620.

Flaskos, J. (2012). The developmental neurotoxicity of organophosphorus insecticides: A direct role for the oxon metabolites. *Toxicol. Lett.* **209**, 86–93.

Frank, C. L., Brown, J. P., Wallace, K., Mundy, W. R., and Shafer, T. J. (2017). From the cover: Developmental neurotoxicants disrupt activity in cortical networks on microelectrode arrays: Results of screening 86 compounds during neural network formation. *Toxicol. Sci.* **160**, 121–135.

Galvez, T., Urwyler, S., Prézeau, L., Mosbacher, J., Joly, C., Malitschek, B., Heid, J., Brabet, I., Froestl, W., Bettler, B., *et al.* (2000). Ca(2+) requirement for high-affinity gamma-aminobutyric acid (GABA) binding at GABA(B) receptors: Involvement of serine 269 of the GABA(B)R1 subunit. *Mol. Pharmacol.* **57**, 419–426.

Gao, H. M., Hong, J.-S., Zhang, W., and Liu, B. (2002). Distinct role for microglia in rotenone-induced degeneration of dopaminergic neurons. *J. Neurosci.* **22**, 782–790.

Goldsmith, D. R., Wagstaff, A. J., Ibbotson, T., and Perry, C. M. (2003). Lamotrigine: A review of its use in bipolar disorder. *Drugs* **63**, 2029–2050.

Grimm, F. A., Iwata, Y., Sirenko, O., Bittner, M., and Rusyn, I. (2015). High-content assay multiplexing for toxicity screening in induced pluripotent stem cell-derived cardiomyocytes and hepatocytes. *Assay Drug Dev. Technol.* **13**, 529–546.

Harrill, J. A., Robinette, B. L., Freudenrich, T., and Mundy, W. R. (2013). Use of high content image analyses to detect chemical-mediated effects on neurite sub-populations in primary rat cortical neurons. *Neurotoxicology* **34**, 61–73.

Hartley, B. J., and Brennand, K. J. (2016). Neural organoids for disease phenotyping, drug screening and developmental biology studies. *Neurochem. Int.* **106**, 85–93.

Hassenklöver, T., Predehl, S., Pilli, J., Ledwolorz, J., Assmann, M., and Bickmeyer, U. (2006). Bromophenols, both present in marine organisms and in industrial flame retardants, disturb cellular Ca2+ signaling in neuroendocrine cells (PC12). *Aquat. Toxicol.* **76**, 37–45.

Hendriks, H. S., van Kleef, R. G. D. M., van den Berg, M., and Westerink, R. H. S. (2012). Multiple novel modes of action involved in the *in vitro* neurotoxic effects of tetrabromobisphenol-A. *Toxicol. Sci.* **128**, 235–246.

Hendriks, H. S., and Westerink, R. H. (2015). Neurotoxicity and risk assessment of brominated and alternative flame retardants. *Neurotoxicol. Teratol.* **52**, 248–269.

Heusinkveld, H. J., Thomas, G. O., Lamot, I., van den Berg, M., Kroese, A. B., and Westerink, R. H. (2010). Dual actions of lindane (gamma-hexachlorocyclohexane) on calcium homeostasis and exocytosis in rat PC12 cells. *Toxicol. Appl. Pharmacol.* **248**, 12–19.

Huettner, J. E., and Bean, B. P. (1988). Block of N-methyl-D-aspartate-activated current by the anticonvulsant MK-801: Selective binding to open channels. *Proc. Natl. Acad. Sci. U.S.A.* **85**, 1307–1311.

Jarema, K.A., Hunter, D.L., Shaffer, R.M., Behl, M., Padilla, S. (2015). Acute and developmental behavioral effects of flame retardants and related chemicals in zebrafish. *Neurotoxicology and Teratology* **52**, 194–209.

Jang, Y., Lee, A. Y., Jeong, S. H., Park, K. H., Paik, M. K., Cho, N. J., Kim, J. E., and Cho, M. H. (2015). Chlorpyrifos induces NLRP3 inflammasome and pyroptosis/apoptosis via mitochondrial oxidative stress in human keratinocyte HaCaT cells. *Toxicology* **338**, 37–46.

Jordan, M. A., and Wilson, L. (2004). Microtubules as a target for anticancer drugs. *Nat. Rev. Cancer* **4**, 253–265.

Jorfi, M., D'Avanzo, C., Tanzi, R. E., Kim, D. Y., and Irimia, D. (2018). Human neurospheroid arrays for *in vitro* studies of Alzheimer's disease. *Sci. Rep.* **8**, 2450–2463.

Judson, R., Richard, A., Dix, D. J., Houck, K., Martin, M., Kavlock, R., Dellarco, V., Henry, T., Holderman, T., Sayre, P., *et al.* (2009a). The toxicity data landscape for environmental chemicals. *Environ. Health Perspect.* **117**, 685–695.

Judson, R. S., Houck, K. A., Kavlock, R. J., Knudsen, T. B., Martin, M. T., Mortensen, H. M., Reif, D. M., Rotroff, D. M., Shah, I., Richard, A. M., *et al.* (2009b). *In vitro* screening of environmental chemicals for targeted testing prioritization: The ToxCast project. *Environ. Health Perspect.* **118**, 485–492.

Kaufman, J. D., Morgan, M. S., Marks, M. L., Greene, H. L., and Rosenstock, L. (1992). A study of the cardiac effects of bromochlorodifluoromethane (halon 1211) exposure during exercise. *Am. J. Ind. Med.* **21**, 223–233.

Kelm, J. M., and Fussenegger, M. (2004). Microscale tissue engineering using gravity-enforced cell assembly. *Trends Biotechnol.* **22**, 195–202.

Khademhosseini, A., Langer, R., Borenstein, J., and Vacanti, J. P. (2006). Microscale technologies for tissue engineering and biology. *Proc. Natl. Acad. Sci. U.S.A.* **103**, 2480–2487.

Kijanska, M., and Kelm, J. (2004). *In vitro* 3D spheroids and microtissues: ATP-based cell viability and toxicity assays. In *Assay Guidance Manual* (G. S. Sittampalam, N. P. Coussens, K. Brimacombe, A. Grossman, M. Arkin, D. Auld, C. Austin, J. Baell, B. Bejcek, and J. M. M. Caaveiro, Eds.), pp. 1–16. Eli Lilly & Company and the National Center for Advancing Translational Sciences, Bethesda, MD.

King, T. S., Potter, D., Kang, I. S., Norris, C., Chen, E., Schenken, R. S., and Javors, M. A. (1999). Concentration-dependent effects of muscimol to enhance pulsatile GnRH release from GT1-7 neurons *in vitro*. *Brain Res.* **824**, 56–62.

Krug, A.K., Balmer, N.V., Matt, F., Schönenberger, F., Merhof, D., Leist, M. (2013). Evaluation of a human neurite growth assay as specific screen for developmental neurotoxicants. *Arch Toxicol.* **87**, 2215–2231.

Kuijlaars, J., Oyelami, T., Diels, A., Rohrbacher, J., Versweyveld, S., Meneghello, G., Tuefferd, M., Verstraelen, P., Detrez, J. R., Verschuuren, M., *et al.* (2016). Sustained synchronized neuronal network activity in a human astrocyte co-culture system. *Sci. Rep.* **6**, 36529.

Kunz-Schughart, L. A., Freyer, J. P., Hofstaedter, F., and Ebner, R. (2004). The use of 3-D cultures for high-throughput screening: The multicellular spheroid model. *J. Biomol. Screen.* **9**, 273–285.

Lancaster, M. A., and Knoblich, J. A. (2014). Generation of cerebral organoids from human pluripotent stem cells. *Nat. Protoc.* **9**, 2329–2340.

Langer, R., and Tirrell, D. A. (2004). Designing materials for biology and medicine. *Nature* **428**, 487–492.

Larm, J. A., Cheung, N. S., and Beart, P. M. (1996). (S)-5-fluorowillardiine-mediated neurotoxicity in cultured murine cortical neurones occurs via AMPA and kainate receptors. *Eur. J. Pharmacol.* **314**, 249–254.

Lee, S. H., Govindaiah, G., and Cox, C. L. (2010). Selective excitatory actions of DNQX and CNQX in rat thalamic neurons. *J. Neurophysiol.* **103**, 1728–1734.

Lee, C. C., and Peters, P. J. (1976). Neurotoxicity and behavioral effects of thiram in rats. *Environ. Health Perspect.* **17**, 35–43.

Lema, S. C., Schultz, I. R., Scholz, N. L., Incardona, J. P., and Swanson, P. (2007). Neural defects and cardiac arrhythmia in fish larvae following embryonic exposure to 2, 2′, 4, 4′-tetrabromodiphenyl ether (PBDE 47). *Aquat. Toxicol.* **82**, 296–307.

Li, B. X., Yang, B. F., Zhou, J., Xu, C. Q., and Li, Y. R. (2001). Inhibitory effects of berberine on IK1, IK, and HERG channels of cardiac myocytes. *Acta Pharmacol. Sin.* **22**, 125–131.

Login, I. S., Pal, S. N., Adams, D. T., and Gold, P. E. (1998). Muscimol increases acetylcholine release by directly stimulating adult striatal cholinergic interneurons. *Brain Res.* **779**, 33–40.

Luo, C., Lancaster, M. A., Castanon, R., Nery, J. R., Knoblich, J. A., and Ecker, J. R. (2016). Cerebral organoids recapitulate epigenomic signatures of the human fetal brain. *Cell Rep.* **17**, 3369–3384.

Magi, S., Castaldo, P., Macrì, M. L., Maiolino, M., Matteucci, A., Bastioli, G., Gratteri, S., Amoroso, S., and Lariccia, V. (2016). Intracellular calcium dysregulation: Implications for Alzheimer's disease. *Biomed. Res. Int.* **2016**, 1. ID 6701324, 14 pages.

Marchan, R., van Thriel, C., and Bolt, H. M. (2013). Recent developments in *in vitro* toxicology: Perspectives of European research and Tox21. *Arch. Toxicol.* **87**, 2043–2046.

Martinez, C., Sanchez, M., Hidalgo, A., and Garcia de Boto, M. J. (2001). Involvement of K(ATP) channels in diethylstilbestrol-induced relaxation in rat aorta. *Eur. J. Pharmacol.* **413**, 109–116.

McCool, B. A., Frye, G. D., Pulido, M. D., and Botting, S. K. (2003). Effects of chronic ethanol consumption on rat GABA(A) and strychnine-sensitive glycine receptors expressed by lateral/basolateral amygdala neurons. *Brain Res.* **963**, 165–177.

Meijer, M., Brandsema, J. A. R., Nieuwenhuis, D., Wijnolts, F. M. J., Dingemans, M. M. L., and Westerink, R. H. S. (2015). Inhibition of voltage-gated calcium channels after subchronic and repeated exposure of PC12 cells to different classes of insecticides. *Toxicol. Sci.* **147**, 607–617.

Mordwinkin, N. M., Burridge, P. W., and Wu, J. C. (2013). A review of human pluripotent stem cell-derived cardiomyocytes for high-throughput drug discovery, cardiotoxicity screening, and publication standards. *J. Cardiovasc. Transl. Res.* **6**, 22–30.

Narahashi, T. (1996). Neuronal ion channels as the target sites of insecticides. *Pharmacol. Toxicol.* **79**, 1–14.

Ogata, N., Vogel, S. M., and Narahashi, T. (1988). Lindane but not deltamethrin blocks a component of GABA-activated chloride channels. *FASEB J.* **2**, 2895–2900.

Pacico, N., and Mingorance-Le Meur, A. (2014). New *in vitro* phenotypic assay for epilepsy: Fluorescent measurement of synchronized neuronal calcium oscillations. *PLoS One* **9**, e84755.

Pérez-Gómez, A., Cabrera-García, D., Warm, D., Marini, A. M., Salas Puig, J., Fernández-Sánchez, M. T., and Novelli, A. (2018). From the cover: Selective enhancement of domoic acid toxicity in primary cultures of cerebellar granule cells by lowering extracellular Na+ concentration. *Toxicol. Sci.* **161**, 103–114.

Qin, X. Y., Akanuma, H., Wei, F., Nagano, R., Zeng, Q., Imanishi, S., Ohsako, S., Yoshinaga, J., Yonemoto, J., Tanokura, M., *et al.* (2012). Effect of low-dose thalidomide on dopaminergic neuronal differentiation of human neural progenitor cells: A combined study of metabolomics and morphological analysis. *Neurotoxicology* **33**, 1375–1380.

Robinson, H. P., Kawahara, M., Jimbo, Y., Torimitsu, K., Kuroda, Y., Kawana, A. (1993). Periodic synchronized bursting and intracellular calcium transients elicited by low magnesium in cultured cortical neurons. *J Neurophysiol.* **70**, 1606–1616.

Radio, N. M., and Mundy, W. R. (2008). Developmental neurotoxicity testing *in vitro*: Models for assessing chemical effects on neurite outgrowth. *Neurotoxicology* **29**, 361–376.

Ramsden, D., Tweedie, D. J., Chan, T. S., Taub, M. E., and Li, Y. (2014). Bridging *in vitro* and *in vivo* metabolism and transport of faldaprevir in human using a novel cocultured human hepatocyte system, HepatoPac. *Drug Metab. Dispos.* **42**, 394–406.

Regan, R. F. (1996). The vulnerability of spinal cord neurons to excitotoxic injury: Comparison with cortical neurons. *Neurosci. Lett.* **213**, 9–12.

Reif, D. M., Sypa, M., Lock, E. F., Wright, F. A., Wilson, A., Cathey, T., Judson, R. R., and Rusyn, I. (2013). ToxPi GUI: An interactive visualization tool for transparent integration of data from diverse sources of evidence. *Bioinformatics* **29**, 402–403.

Renner, M., Lancaster, M. A., Bian, S., Choi, H., Ku, T., Peer, A., Chung, K., and Knoblich, J. A. (2017). Self-organized developmental patterning and differentiation in cerebral organoids. *EMBO J.* **36**, 1316–1329.

Ryan, K. R., Sirenko, O., Parham, F., Hsieh, J. H., Cromwell, E. F., Tice, R. R., and Behl, M. (2016). Neurite outgrowth in human induced pluripotent stem cell-derived neurons as a high-throughput screen for developmental neurotoxicity or neurotoxicity. *Neurotoxicology* **53**, 271–281.

Seeman, P. (2002). Atypical antipsychotics: Mechanism of action. *Can. J. Psychiatry* **47**, 27–38.

Shafer, T. J., and Meyer, D. A. (2004). Effects of pyrethroids on voltage-sensitive calcium channels: A critical evaluation of strengths, weaknesses, data needs, and relationship to assessment of cumulative neurotoxicity. *Toxicol. Appl. Pharmacol.* **196**, 303–318.

Sheets, M. F., and Hanck, D. A. (2003). Molecular action of lidocaine on the voltage sensors of sodium channels. *J. Gen. Physiol.* **121**, 163–175.

Sheu, S. S., and Lederer, W. J. (1985). Lidocaine's negative inotropic and antiarrhythmic actions. Dependence on shortening of action potential duration and reduction of intracellular sodium activity. *Circ. Res.* **57**, 578–590.

Shew, W. L., Bellay, T., and Plenz, D. (2010). Simultaneous multi-electrode array recording and two-photon calcium imaging of neural activity. *J. Neurosci. Methods* **192**, 75–82.

Sinnecker, D., Laugwitz, K.-L., and Moretti, A. (2014). Induced pluripotent stem cell-derived cardiomyocytes for drug development and toxicity testing. *Pharmacol. Ther.* **143**, 246–252.

Sirenko, O., Crittenden, D., Callamaras, N., Hesley, J., Chen, Y.-W., Funes, C., Rusyn, I., Anson, B., and Cromwell, E. F. (2013b). Multiparameter *in vitro* assessment of compound effects on cardiomyocyte physiology using iPSC cells. *J. Biomol. Screen.* **18**, 39–53.

Sirenko, O., Cromwell, E. F., Crittenden, C., Wignall, J. A., Wright, F. A., and Rusyn, I. (2013a). Assessment of beating parameters in human induced pluripotent stem cells enables quantitative *in vitro* screening for cardiotoxicity. *Toxicol. Appl. Pharmacol.* **273**, 500–507.

Sirenko, O., Grimm, F. A., Ryan, K. R., Iwata, Y., Chiu, W. A., Parham, F., Wignall, J. A., Anson, B., Cromwell, E. F., Behl, M., *et al.* (2017). *In vitro* cardiotoxicity assessment of environmental chemicals using an organotypic human induced pluripotent stem cell-derived model. *Toxicol. Appl. Pharmacol.* **322**, 60–74.

Sirenko, O., Hancock, M. K., Hesley, J., Dihui, H., Avrum, C., Jason, G., Carlson, C. B., and Mann, D. (2016). Phenotypic characterization of toxic compound effects on liver spheroids derived from iPSC using confocal imaging and three-dimensional image analysis. *Assay Drug Dev. Technol.* **14**, 381–394.

Sirenko, O., Mitlo, T., Hesley, J., Luke, S., Owens, W., and Cromwell, E. F. (2015). High-content assays for characterizing the viability and morphology of 3D cancer spheroid cultures. *Assay Drug Dev. Technol.* **13**, 402–414.

Smetters, D., Majewska, A., and Yuste, R. (1999). Detecting action potentials in neuronal populations with calcium imaging. *Methods* **18**, 215–221.

Soderlund, D. M., Clark, J. M., Sheets, L. P., Mullin, L. S., Piccirillo, V. J., Sargent, D., Stevens, J. T., and Weiner, M. L. (2002). Mechanisms of pyrethroid neurotoxicity: Implications for cumulative risk assessment. *Toxicology* **171**, 3–59.

Suter-Dick, L., Alves, P. M., Blaauboer, B. J., Bremm, K.-D., Brito, C., Coecke, S., Flick, B., Fowler, P., Hescheler, J., Ingelman-Sundberg, M., *et al.* (2015). Stem cell-derived systems in toxicology assessment. *Stem Cells Dev.* **24**, 1284–1296.

Tang, Y., Donnelly, K. C., Tiffany-Castiglioni, E., and Mumtaz, M. M. (2003). Neurotoxicity of polycyclic aromatic hydrocarbons and simple chemical mixtures. *J. Toxicol. Environ. Health A* **66**, 919–940.

Tice, R. R., Austin, C. P., Kavlock, R. J., and Bucher, J. R. (2013). Improving the human hazard characterization of chemicals: A Tox21 update. *Environ. Health Perspect.* **121**, 756–765.

Travis, L. B., Fossa, S. D., Sesso, H. D., Frisina, R. D., Herrmann, D. N., Beard, C. J., Feldman, D. R., Pagliaro, L. C., Miller, R. C., Vaughn, D. J., *et al.* (2014). Chemotherapy-induced peripheral neurotoxicity and ototoxicity: New paradigms for translational genomics. *J. Natl. Cancer Inst.* **106**, dju044.

Valdivia, P., Martin, M., LeFew, W. R., Ross, J., Houck, K. A., and Shafer, T. J. (2014). Multi-well microelectrode array recordings detect neuroactivity of ToxCast compounds. *NeuroToxicology* **44**, 204–217.

Vargesson, N. (2015). Thalidomide-induced teratogenesis: History and mechanisms. *Birth Defects Res. C: Embryo Today* **105**, 140–156.

Verstraelen, P., Pintelon, I., Nuydens, R., Cornelissen, F., Meert, T., and Timmermans, J.-P. (2014). Pharmacological characterization of cultivated neuronal networks: Relevance to synaptogenesis and synaptic connectivity. *Cell. Mol. Neurobiol.* **34**, 757–776.

Vogel, S., and Sperelakis, N. (1978). Valinomycin blockade of myocardial slow channels is reversed by high glucose. *Am. J. Physiol.* **235**, H46–H51.

Vorhees, C. V., Weisenburger, W. P., and Minck, D. R. (2001). Neurobehavioral teratogenic effects of thalidomide in rats. *Neurotoxicol. Teratol.* **23**, 255–264.

Wambaugh, J. F., Wetmore, B. A., Pearce, R., Strope, C., Goldsmith, R., Sluka, J. P., Sedykh, A., Tropsha, A., Bosgra, S., Shah, I., *et al.* (2015). Toxicokinetic triage for environmental chemicals. *Toxicol. Sci.* **147**, 55–67.

Wang, X., and Gruenstein, E. I. (1997). Mechanism of synchronized Ca^{2+} oscillations in cortical neurons. *Brain Res.* **767**, 239–249.

Whitehouse, P. J., Price, D. L., Struble, R. G., Clark, A. W., Coyle, J. T., and Delon, M. R. (1982). Alzheimer's disease and senile dementia: Loss of neurons in the basal forebrain. *Science* **215**, 1237–1239.

Wignall, J. A., Shapiro, A. J., Wright, F. A., Woodruff, T. J., Chiu, W. A., Guyton, K. Z., and Rusyn, I. (2014). Standardizing benchmark dose calculations to improve science-based decisions in human health assessments. *Environ. Health Perspect.* **122**, 499–505.

Wijdicks, E. F. (2001). Neurotoxicity of immunosuppressive drugs. *Liver Transpl.* **7**, 937–942.

Wong, R. O. (1998). Calcium imaging and multielectrode recordings of global patterns of activity in the developing nervous system. *Histochem. J.* **30**, 217–229.

Wong, E. H., Kemp, J. A., Priestley, T., Knight, A. R., Woodruff, G. N., and Iversen, L. L. (1986). The anticonvulsant MK-801 is a potent N-methyl-D-aspartate antagonist. *Proc. Natl. Acad. Sci. U.S.A.* **83**, 7104–7108.

Yan, M., Zhang, K., Shi, Y., Fent, L., Lv, L., and Li, B. (2015). Mechanism and pharmacological rescue of berberine-induced hERG channel deficiency. *Drug Des. Dev. Ther.* **9**, 5737–5747.

Zafar, S. N., Khan, A. A., Ghauri, A. A., and Shamim, M. S. (2012). Phenytoin versus Levetiracetam for seizure prophylaxis after brain injury—A meta analysis. *BMC Neurol.* **12**, 30.

Zafiropoulos, A., Tsarouhas, K., Tsitsimpikou, C., Fragkiadaki, P., Germanakis, I., Tsardi, M., Maravgakis, G., Goutzourelas, N., Vasilaki, F., Kouretas, D., *et al.* (2014). Cardiotoxicity in rabbits after a low-level exposure to diazinon, propoxur, and chlorpyrifos. *Hum. Exp. Toxicol.* **33**, 1241–1252.

Zhang, Y., Huang, L., Zuo, Z., Chen, Y., and Wang, C. (2013). Phenanthrene exposure causes cardiac arrhythmia in embryonic zebrafish via perturbing calcium handling. *Aquat. Toxicol.* **142–143**, 26–32.

Zhao, F., Li, X., Jin, L., Zhang, F., Inoue, M., Yu, B., and Cao, Z. (2016). Development of a rapid throughput assay for identification of hNav1.7 antagonist using unique efficacious sodium channel agonist, antillatoxin. *Mar. Drugs* **14**, 36.